Human-Inspired Neuro-Symbolic World Modeling and Logic Reasoning for Interpretable Safe UAV Landing Site Assessment

Weixian Qian
Macquarie University
Sydney, Australia
weixian.qian@mq.edu.au

Tianyi Yang
University of California, Santa Barbara
Santa Barbara, USA
tianyi_yang@ucsb.edu

Sebastian Schroder
Macquarie University
Sydney, Australia
sebastian.schroder@mq.edu.au

Yao Deng
Macquarie University
Sydney, Australia
yao.deng@anitron.com

Jiaohong Yao
Macquarie University
Sydney, Australia
jiaohong.yao@hdr.mq.edu.au

Xiao Cheng
Macquarie University
Sydney, Australia
xiao.cheng@mq.edu.au

Richard Han
Macquarie University
Sydney, Australia
richard.han@mq.edu.au

Xi Zheng
Macquarie University
Sydney, Australia
james.zheng@mq.edu.au

Abstract

Reliable assessment of safe landing sites in unstructured environments is essential for deploying Unmanned Aerial Vehicles (UAVs) in real-world applications such as delivery, inspection, and surveillance. Existing learning-based approaches often degrade under covariate shift and offer limited transparency, making their decisions difficult to interpret and validate on resource-constrained platforms. We present NeuroSymLand, a neuro-symbolic framework for marker-free UAV landing site safety assessment that explicitly separates perception-driven world modeling from logic-based safety reasoning. A lightweight segmentation model incrementally constructs a probabilistic semantic scene graph encoding objects, attributes, and spatial relations. Symbolic safety rules, synthesized offline via large language models with human-in-the-loop refinement, are executed directly over this world model at runtime to perform white-box reasoning, producing ranked landing candidates with human-readable explanations of the underlying safety constraints. Across 72 simulated and hardware-in-the-loop landing scenarios, NeuroSymLand achieves **61 successful assessments**, outperforming four competitive baselines, which achieve between 37 and 57 successes. Qualitative analysis highlights its superior interpretability and transparent reasoning, while deployment incurs negligible edge overhead. Our results suggest that combining explicit world modeling with symbolic reasoning can support accurate, interpretable, and edge-deployable safety assessment in mobile systems, as demonstrated through UAV landing site assessment.

Conference acronym 'XX, Woodstock, NY

ACM ISBN 978-1-4503-XXXX-X/2018/06
https://doi.org/XXXXXXX.XXXXXXX

CCS Concepts

• **Human-centered computing** → **Ubiquitous and mobile computing systems and tools**; **Ubiquitous and mobile computing**; **Human computer interaction (HCI)**; **Ubiquitous and mobile computing systems and tools**; **Ubiquitous and mobile computing systems and tools**; • **Software and its engineering** → *Software design engineering*; *Software design engineering*; *Software design engineering*; • **Computer systems organization** → **Embedded and cyber-physical systems**; **Real-time systems**; • **Computing methodologies** → **Symbolic and algebraic manipulation**; **Knowledge representation and reasoning**; **Spatial and physical reasoning**.

Keywords

Neurosymbolic reasoning, Unmanned Aerial Vehicle (UAV)

ACM Reference Format:
Weixian Qian, Tianyi Yang, Sebastian Schroder, Yao Deng, Jiaohong Yao, Xiao Cheng, Richard Han, and Xi Zheng. 2018. Human-Inspired Neuro-Symbolic World Modeling and Logic Reasoning for Interpretable Safe UAV Landing Site Assessment. In *Proceedings of Make sure to enter the correct conference title from your rights confirmation email (Conference acronym 'XX).* ACM, New York, NY, USA, 19 pages. https://doi.org/XXXXXXX.XXXXXXX

1 INTRODUCTION

Unmanned Aerial Vehicles (UAVs) [17, 32, 59] are increasingly expected to operate in close proximity to people and critical infrastructure, where landing represents the most safety-critical phase of a mission. A single misjudgment of a landing site can endanger bystanders, damage the airframe, or harm nearby assets. As a result, *landing site assessment* (LSA) has attracted growing attention. While much prior work frames the problem as landing site detection, we argue that safe UAV operation in public and unstructured environments fundamentally requires *context-aware* LSA, in which safety judgments depend not only on geometric and visual cues but also on semantic and situational context, such as nearby people

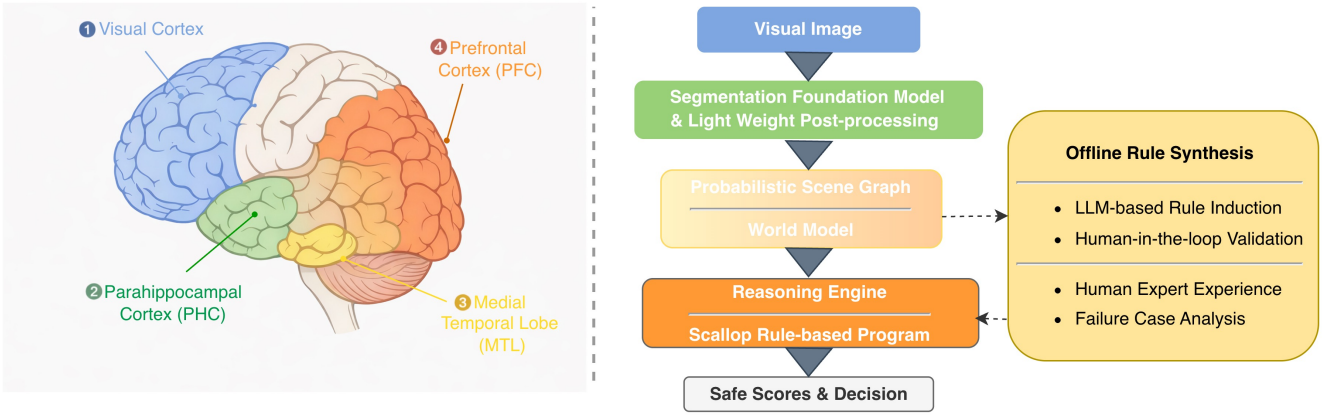

Figure 1: Functional correspondence between brain systems (left) and a perception–world modeling–reasoning architecture with offline cognitive control (right).

and facilities, environmental affordances, and time-dependent or mission-specific constraints.

Despite steady progress, most marker-free LSA pipelines [25, 52, 53, 55] remain dominated by deep learning approaches that estimate landing feasibility from geometric properties (e.g., flatness, slope, roughness) and coarse semantic cues (e.g., vegetation, vehicles, people). While effective at identifying obvious hazards, these models typically provide limited interpretability and exhibit weak compositional generalization under covariate shift. More importantly, they rarely expose higher-level contextual semantics or verifiable rules that are essential for certification, regression testing, and safety case construction [49]. For example, constraints such as "$\forall$ construction zone $\cap$ crane $\rightarrow$ unsafe" or "$\forall$ place $\in$ {school, station} $\cap$ operating hours $\rightarrow$ unsafe" are natural to human operators, yet difficult to express, inspect, or update in end-to-end predictors. As a result, perception and decision logic are often entangled in opaque models, limiting transparency and hindering principled safety validation. Recent LLM- and VLM-based approaches [3, 9, 30] attempt to inject higher-level reasoning into perception pipelines, but typically rely on implicit prompting or black-box inference, making their decision boundaries difficult to verify and their behavior under distribution shift hard to control.

Compounding these challenges, LSA objectives are inherently mission dependent. Emergency landings [16, 37] prioritize rapid risk reduction, rescue operations [5, 19, 39] balance accessibility and proximity to casualties, while delivery missions [11, 21, 33] impose strict geofencing and strong protections for bystanders and property. Nevertheless, most existing pipelines remain largely scenario agnostic, since adapting decision logic typically requires retraining perception models or redesigning task-specific heuristics. This tight coupling limits the ability to provide transparent justifications and formally checkable go/no-go decisions, even though human pilots routinely assess landing safety by reasoning over explicit contextual constraints and mission rules.

Figure 1 illustrates the neuroscience-inspired motivation behind our architectural separation by juxtaposing key brain systems (left) with the corresponding stages in our computational pipeline (right). On the left, context-guided behavior in humans emerges from a progression of processing stages spanning visual perception, contextual representation, memory, and cognitive control. Early visual cortex extracts local visual features, while the parahippocampal cortex (PHC), a major component of the medial temporal lobe (MTL), integrates these features into scene-level and contextual representations that capture spatial layout and environmental semantics. These representations are maintained and structured through interactions within the broader MTL and subsequently influence decision-making and control processes in the prefrontal cortex (PFC), which applies abstract rules, goals, and constraints to guide behavior [6, 48].

The right side of the figure mirrors this functional organization in a modular computational design. Visual input is first processed by a lightweight segmentation foundation model and post-processing pipeline, corresponding to early visual processing. The resulting probabilistic semantic scene graph serves as an MTL-inspired world model, encoding scene-scale structure, spatial relations, and uncertainty in a form that can be incrementally updated online. Crucially, safety reasoning is not embedded within the perception model itself. Instead, inspired by the role of the PFC, safety logic is constructed offline through LLM-assisted rule synthesis with human-in-the-loop validation, distilling expert knowledge, failure analyses, and mission-specific constraints into reusable symbolic programs. At runtime, these pre-validated rules are executed by a reasoning engine directly over the world model, producing calibrated safety scores and auditable decisions. This explicit separation between online world modeling and offline reasoning construction reflects both the differing timescales and representational roles observed in human cognition and enables interpretable, verifiable, and mission-adaptive landing site assessment without retraining the perception stack.

Concretely, NeuroSymLand implements this separation through a three-stage pipeline spanning perception, rule construction, and runtime execution. Semantic segmentation combined with lightweight geometric post-processing (e.g., contour extraction, connected components, flatness and slope proxies, and short-horizon

temporal smoothing) produces probabilistic Scallop facts that are assembled into a calibrated semantic scene graph encoding spatial and relational structure. Safety logic is constructed offline using a large language model [47] with human-in-the-loop refinement over diverse scenes and synthetic edge cases, and compiled into probabilistic first-order predicates. At runtime, these pre-validated rules execute directly over the scene graph as a white-box safety gate, producing calibrated safety scores and auditable go/no-go assessments. Mission-aware rule packs (e.g., emergency, rescue, delivery) can be swapped or updated at runtime, enabling rapid adaptation without retraining or modifying the perception stack.

Contributions. This paper makes the following contributions:

- **Neuroscience-inspired neuro-symbolic architecture.** We introduce a principled separation between online world modeling and offline reasoning construction, inspired by complementary roles of the MTL and PFC, enabling interpretable and reusable safety reasoning for marker-free UAV landing site assessment.
- **Offline rule synthesis with human oversight.** We present an LLM-assisted, human-in-the-loop rule synthesis pipeline that distills expert knowledge, failure cases, and mission constraints into verifiable Scallop programs compiled as probabilistic first-order logic.
- **Online, edge-ready reasoning over world models.** We combine an INT8-quantized foundation segmentation model with lightweight geometric processing to construct a probabilistic semantic scene graph over which pre-validated rules execute as a white-box safety gate, enabling mission reconfiguration without retraining.
- **Comprehensive evaluation.** Through software-in-the-loop (SIL) and hardware-in-the-loop (HIL) experiments, we demonstrate that NeuroSymLand achieves improved landing site assessment quality and substantially greater interpretability than competing LSA baselines, while operating within tight compute and memory budgets on embedded edge hardware and producing explicit, inspectable reasoning traces for each decision.

The paper is organized as follows: Section 2 reviews related work, Section 3 presents our methodology, Section 4 reports experimental setup and results, and Section 5 concludes with future directions.

2 Related Work

2.1 UAV Landing Site Assessment

Landing site assessment (LSA) has historically included both marker-based and markerless approaches. Marker-based pipelines rely on reference markers such as AprilTag [46, 56] or ArUco [24], but are increasingly impractical in real deployments due to instrumentation cost and brittleness under glare, occlusion, and adverse weather. Markerless LSA instead infers landing feasibility directly from onboard sensing without pre-installed infrastructure. **Deep learning–based LSA** methods dominate current markerless pipelines and estimate landing feasibility from geometric cues (e.g., flatness, slope, roughness, clearance) and semantic vetoes (e.g., people, vehicles, water) [25, 52, 53, 55]. Recent perception-centric systems extend this direction with depth-based terrain reasoning for GPS-denied flight [15], active depth sensing with collision avoidance using gimbaled depth cameras [38], and integrated emergency landing pipelines that combine SLAM, object detection, and occupancy mapping under time-critical constraints [42]. Beyond static sites, landing on moving platforms has been addressed by explicitly modeling platform-induced aerodynamics [22] and by event-based optic-flow guidance with adaptive Koopman-style dynamics modeling [7]. **LLM-based and vision–language LSA** approaches have recently emerged to inject higher-level contextual reasoning into landing decisions. PEACE automates prompt engineering to improve vision–language segmentation for landing region identification [12]; LLM Land leverages vision–language descriptions and a lightweight LLM to infer context-dependent safety buffers enforced within MPC for replanning [14]; and embodied vision–language agents have been explored for rapid landing decisions under unexpected events [8]. Related security-motivated work further considers LLM-guided landing target selection as part of recovery under cyber attacks [10]. Despite these advances, most existing pipelines do not construct an explicit world model or execute a reasoning engine over such a model. Safety logic is therefore embedded implicitly in task-specific heuristics or learned scores, making decisions difficult to interpret, debug, or modify. The tight coupling between perception and decision-making further limits the ability to express compositional contextual semantics or to inspect and check rule-level behavior, leaving a gap for LSA representations that explicitly separate environment understanding from reasoning and enable transparent, rule-grounded assessment.

2.2 Neuro-Symbolic Reasoning and LLM–Symbolic Integration

Neuro-symbolic (NeSy) approaches aim to combine the representation learning strengths of neural models with the interpretability and structure of symbolic reasoning. Classical NeSy systems typically follow a sequential pipeline, where neural components produce symbolic inputs that are subsequently consumed by a fixed symbolic reasoner. While effective, this loose coupling often limits expressiveness, adaptability, and transparency when reasoning over complex, real-world environments.

Neuro-symbolic and probabilistic logic reasoning Logic programming frameworks such as Prolog [36] provide goal-directed and explainable reasoning, and have been extended to probabilistic and neuro-symbolic settings, including ProbLog [20], DeepProbLog [40], and TensorLog [18]. Scallop [27] advances this line of work by supporting discrete, probabilistic, and differentiable logic programming with provenance semantics, enabling symbolic programs to be executed efficiently on GPUs while remaining inspectable and verifiable. Importantly, Scallop allows reasoning to be performed directly over structured world representations, making it well-suited for decision-making tasks that require explicit rules and traceable outcomes [28].

LLM–symbolic integration and human-in-the-loop reasoning. Recent work has explored using large language models (LLMs) to generate executable symbolic programs or constraints that are then interpreted by external engines or solvers, as demonstrated in robotics and planning systems such as SayCan [4] and Code-as-Policies [34], as well as program-aided reasoning approaches

in QA [23, 58]. These approaches leverage LLMs to distill domain knowledge into symbolic form, but typically treat neural perception, program generation, and symbolic execution as separate sequential stages.

Our tightly integrated neuro-symbolic pipeline. In contrast to prior NeSy approaches that loosely couple neural perception and symbolic reasoning sequentially, we propose a tightly integrated neuro-symbolic pipeline inspired by human reasoning. Foundation models extract rich semantic structure from sensory inputs, producing explicit world models in the form of semantic maps and structured scene representations. An LLM, operating in a human-in-the-loop setting, distills domain expertise into symbolic reasoning code, which is compiled into Scallop programs. At runtime, the reasoning engine is repeatedly executed over the evolving world model, enabling transparent, rule-grounded assessment while keeping perception and reasoning cleanly separated. This design leverages the feature learning power of foundation models for environment understanding and the symbolic expressiveness of Scallop for interpretable and debuggable reasoning, yielding an explicit and auditable neuro-symbolic system.

3 Methodology

Overview. NeuroSymLand is a neuro-symbolic landing site assessment framework that explicitly separates perception from safety reasoning by decoupling online inference from offline rule synthesis. Figure 2 illustrates the online inference stage. Given an input visual image, a frozen and INT8-quantized segmentation backbone (SegFormer-B0), together with lightweight geometric post-processing, lifts pixel-level predictions into region-level evidence, including candidate areas, geometric attributes, and confidence estimates. These region-level outputs are compiled into a probabilistic semantic scene graph that serves as an explicit world model, exposing objects, attributes (e.g., area, flatness), and spatial relations with calibrated probabilities. On top of this world model, a Scallop-based reasoning engine executes an explicit rule library as a white-box safety gate, producing interpretable safety assessments with provenance information. Finally, reasoning results are validated across multiple frames to ensure decision consistency, and a mission-specific ranking function selects the final landing proposal.

Figure 3 provides a structured overview of the *offline reasoning engine construction and refinement workflow*. The figure should be read top-to-bottom and left-to-right. The left branch illustrates how raw image inputs are transformed into an explicit world model (scene graph), after which an LLM synthesizes an initial symbolic reasoning engine from structured prompts. This reasoning engine is executed on top of the world model to produce candidate landing sites, together with rule-trigger traces that are translated into human-readable log insights for expert inspection. The right branch captures the human-in-the-loop refinement cycle, where experts review annotated landing sites and the corresponding top rules triggered by the reasoning process and provide corrective feedback. This feedback is interpreted by a prompt-rewriting module and fed back to the LLM to synthesize a refined reasoning engine, which is re-executed on the same world model to produce updated predictions and explanations. The refinement loop continues until the expert determines that no further feedback is required. The offline workflow is executed independently of online inference and focuses exclusively on synthesizing, validating, and refining executable symbolic safety logic without modifying the perception models or the world-model construction pipeline.

Table 1: Probabilistic scene graph components, aligned with the Semantic Drone Dataset [45].

Semantic Objects	unlabeled, paved area, dirt, grass, gravel, water, rocks, pool, roof, wall, window, door, fence, person, dog, car, bicycle, tree, obstacle
Attributes	is large area, is regular shape, is flat surface, is stable surface, is moving, is smooth surface, is accessible, is safe
Relations	above, bottom, left, right, adjacent_to, contain, on, near_to, far_from, surrounded_by

3.1 Online Generation of Explicit World Models

This subsection details how an explicit probabilistic world model is constructed online from semantic segmentation outputs. As introduced in the Overview, the role of the online pipeline is not to infer safety directly, but to transform visual evidence into a structured, uncertainty-aware representation that can be consumed by the symbolic reasoning engine.

Predefined world-model taxonomy. We predefine the schema of the world model based on a preliminary analysis of a semantic drone dataset [45] and common landing-relevant scene elements. The taxonomy specifies (i) the set of semantic object categories, (ii) node-level attributes, and (iii) spatial relations permitted between entities. This schema is fixed at runtime and shared by both the online inference stage and the offline rule-synthesis process. The complete taxonomy is summarized in Table 1. By fixing the world-model structure a priori, we ensure that perception outputs can be lifted deterministically into symbolic representations and that reasoning rules remain interpretable and auditable.

3.1.1 Perception Backbone and Lightweight Post-processing. Our target platform is an edge device (Jetson Orin Nano Super, 8 GB) operating under strict power, thermal, and memory constraints. To meet these requirements, we restrict online computation to a compact segmentation backbone followed by lightweight, deterministic post-processing routines.

Semantic segmentation. We deploy SegFormer-B0 [57], fine-tuned on the Semantic Drone Dataset [45], and quantized to INT8 for efficient inference. Given an input image, the model produces per-pixel posterior distributions over the predefined semantic object categories listed in Table 1. These dense predictions serve as the sole neural input to world-model construction.

Region extraction, attributes, and spatial relations. Pixel-level posteriors from semantic segmentation are first converted into instance-level regions using standard OpenCV routines [13]. For each semantic class, probability maps are binarized with class-dependent thresholds, followed by contour extraction and connected-component

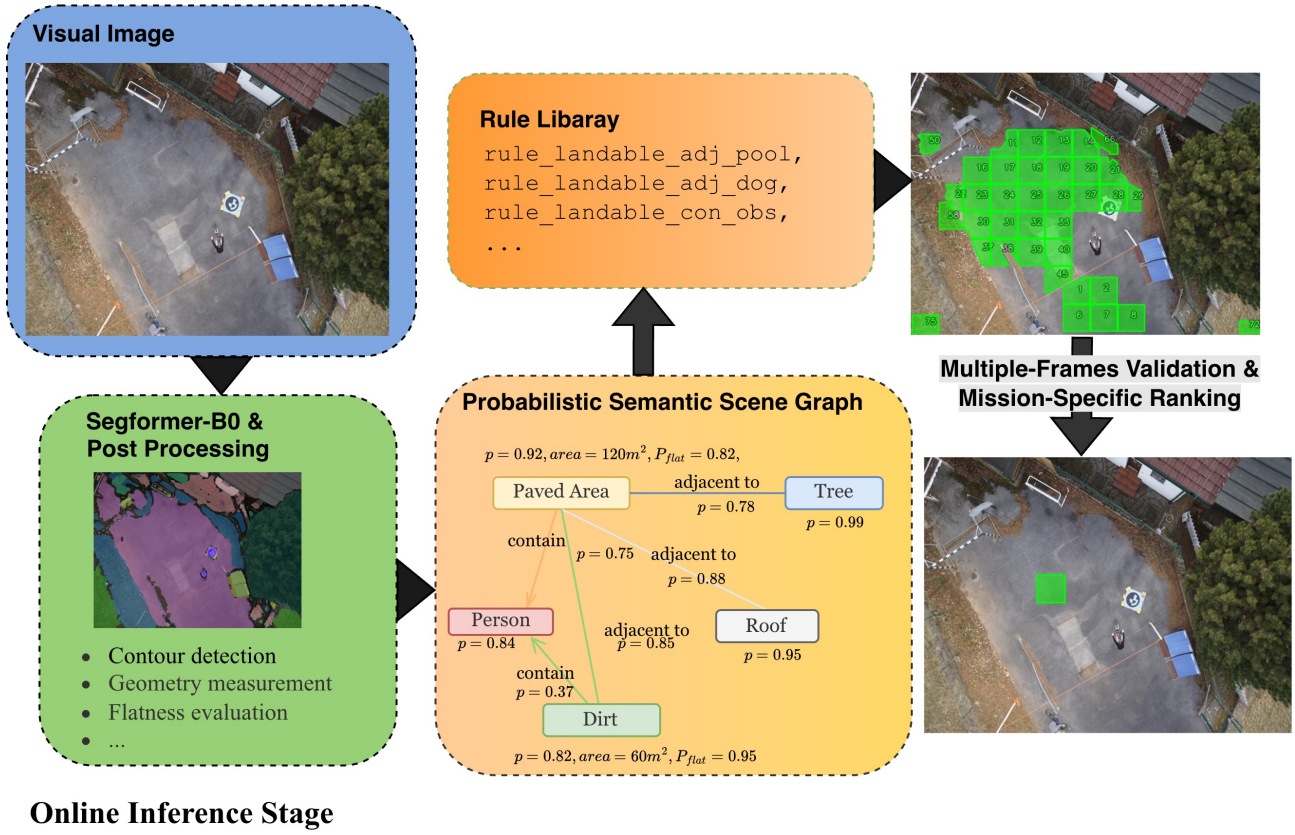

Figure 2: Online inference in NeuroSymLand. Visual inputs are segmented and post processed to construct a probabilistic semantic scene graph. Symbolic safety rules are evaluated over the graph to filter unsafe regions, followed by multi frame validation and mission specific ranking to produce interpretable landing decisions.

analysis. Small contours below a minimum area threshold are discarded to suppress noise, while excessively large regions are optionally split (e.g., via grid- or coverage-based subdivision) to prevent a single dominant instance from biasing downstream relational reasoning. Optionally, polygon simplification is applied to reduce contour complexity.

Each retained region is abstracted as a node in the probabilistic semantic scene graph and is associated with geometric and stability-related attributes, including polygon shape, area, bounding box, centroid, orientation, compactness, and simple flatness and slope proxies derived from local geometry. To reduce sensitivity to transient segmentation noise, attribute estimates are smoothed over a short temporal window of recent frames, yielding a set of tracked regions with calibrated semantic confidence and geometric attributes.

Spatial relations between regions are then constructed deterministically from instance-level geometry. While the taxonomy supports multiple relation types (Table 1), we illustrate the process using three representative examples: *contain*, *adjacent*, and *near-to*. The *contain* relation is derived from the intersection area ratio between two region polygons and mapped through a sigmoid function to obtain a smooth confidence score. The *adjacent* relation is computed based on the minimum distance between polygon boundaries, with logistic or threshold-based mapping and an overlap penalty to avoid misclassifying overlapping regions as adjacent. The *near-to* relation is defined using centroid distance or minimum polygon-to-polygon distance, represented either via distance thresholds or a smoothly decaying probabilistic function.

The resulting instance-level nodes and spatial relations form a directed, probabilistic scene graph, with nodes and edges annotated by calibrated attributes and relation confidences that are directly consumed by the symbolic reasoning engine.

3.1.2 Probabilistic Semantic Scene Graph. We represent the environment using a *Probabilistic Semantic Scene Graph (PSSG)*, which serves as the explicit world model in our framework. The PSSG provides a structured, uncertainty-aware representation that bridges neural perception and symbolic reasoning and is the sole abstraction over which the reasoning engine operates.

Formally, the PSSG is defined as a graph $G = (V, E)$, where each node $v \in V$ corresponds to a connected region extracted from the semantic segmentation output, and each edge $e = (v, u) \in E$ encodes a spatial relation between two regions. The schema of the

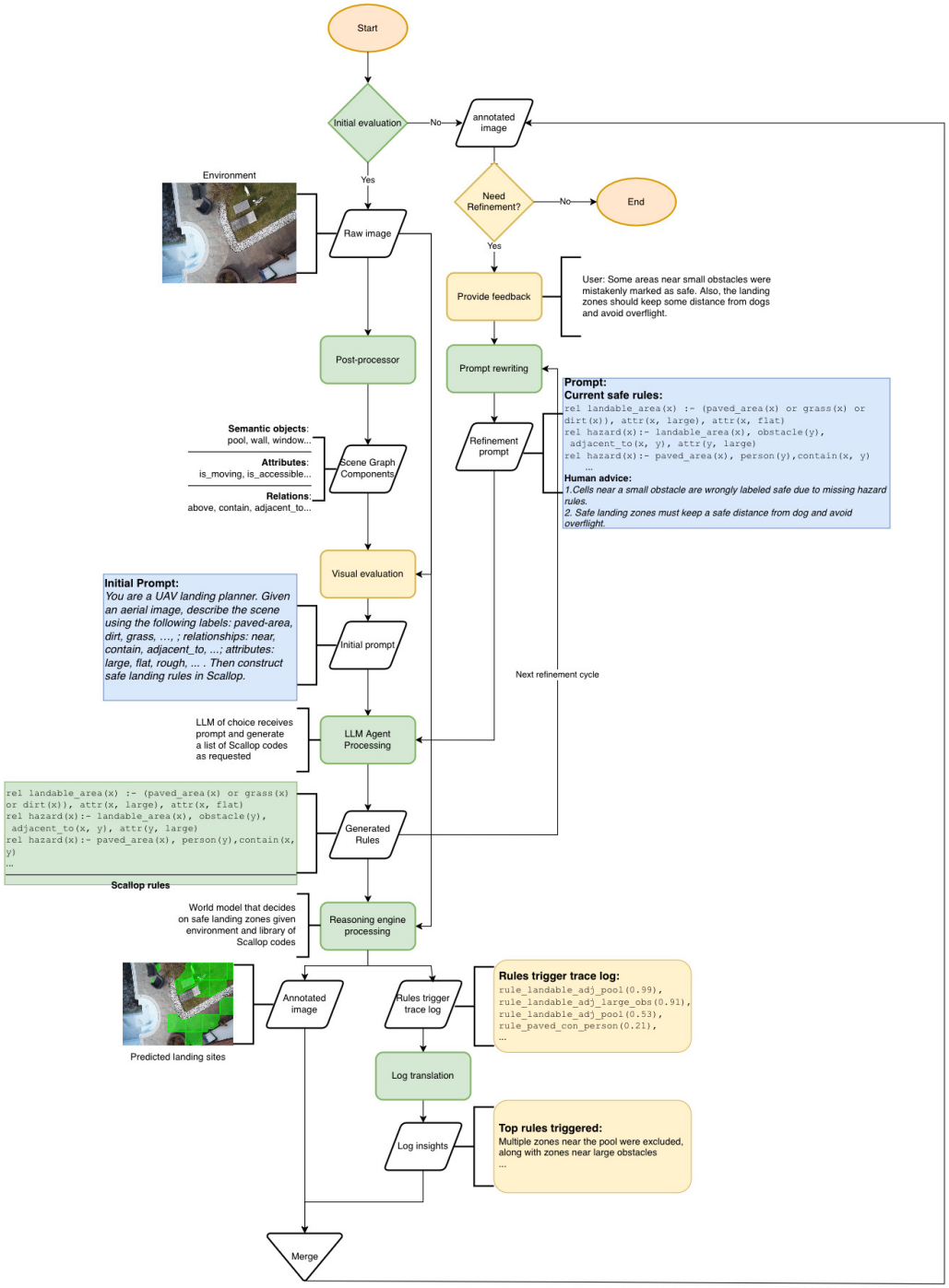

Figure 3: Flow chart for iterative offline rule engine construction with human-in-the-loop refinement. Each round updates the symbolic rule library based on accumulated world model evidence and targeted failure case analysis.

graph-including node types, attributes, and admissible relations-is predefined based on a preliminary study of a semantic drone dataset and is summarized in Table 1.

Node semantics and attributes. Each node in the PSSG carries (i) a probability distribution over semantic object categories and (ii) a calibrated attribute vector defined by the predefined taxonomy. For example, a region may be associated with a high probability of

being a *paved area*, while also exhibiting attributes such as large area, low estimated slope, or high geometric stability. Attributes are represented probabilistically rather than as hard labels, allowing downstream reasoning to account explicitly for uncertainty in perception.

Spatial relations. Edges in the PSSG encode pairwise spatial relations such as adjacency, containment, and proximity. Relation confidences are computed from region geometry and spatial layout, for example using centroid distance, overlap ratios, or boundary adjacency. These relations enable reasoning rules to capture contextual interactions between regions, such as whether a candidate landing area is near obstacles or overlaps with restricted zones.

Probabilistic facts. Let r_i denote a region. For object class c, attribute a, and relation ρ, we denote calibrated confidences by $P_c^{\text{obj}}(i)$, $P_a^{\text{att}}(i)$, and $P_\rho^{\text{rel}}(i,j)$. These quantities are grounded into probabilistic unary and binary predicates, such as paved_area$(i)\,[p]$, is_flat_surface$(i)\,[p]$, and near_to$(i,j)\,[p]$. This grounding lifts dense pixel-level evidence into region-level probabilistic facts whose complexity scales with $|V|$ and $|E|$ rather than image resolution.

Pooling over neighbors. For existential spatial relations (e.g., whether a region is *near* any obstacle), relational evidence is aggregated over neighboring nodes using a t-conorm $\oplus$ (probabilistic sum),

$$\widehat{P}_\rho^{\text{rel}}(i) \;=\; \bigoplus_{j \in \mathcal{N}(i)} P_\rho^{\text{rel}}(i,j), \qquad x \oplus y \equiv 1-(1-x)(1-y).$$

Intuitively, this aggregation captures the probability that region i satisfies relation ρ with *at least one* neighboring region, such as being near to any obstacle, while avoiding sensitivity to the exact number of neighbors. This pooling yields robust region-level relational evidence while preserving calibrated uncertainty, and the resulting values are directly consumed by the symbolic reasoning engine.

Overall, the PSSG constitutes the explicit world model in our system, cleanly separating environment understanding from reasoning and enabling interpretable, rule-grounded landing site assessment.

3.2 Rule-Based Reasoning Engine over the World Model

The core decision component in NeuroSymLand is an explicit, rule-based reasoning engine implemented as a Scallop program [27]. The reasoning engine operates directly on the Probabilistic Semantic Scene Graph (PSSG), which serves as the explicit world model, and infers whether a candidate region is hazardous or safe based on interpretable symbolic rules. In addition to calibrated hazard scores, the engine produces provenance traces that explain which rules and world-model facts contributed to each inference. Rules are organized into a reusable library and can be grouped into mission-specific rule packs.

3.2.1 *Human-in-the-loop reasoning engine construction and refinement.*

Rule synthesis and training data. The reasoning engine is synthesized offline using a curated corpus of 72 landing-site images drawn from the Semantic Drone Dataset [45]. For each image, we construct a PSSG using the same online world-model generation pipeline described in Section 3.1. These PSSGs form structured training instances that expose objects, attributes, and spatial relations in a form directly consumable by symbolic rules.

LLM-driven rule synthesis. Rule induction is formulated as a synthesis task rather than a supervised learning problem. Given a prompt that includes (i) a structured scene description derived from the PSSG, (ii) the current rule library, (iii) curated positive and negative rule templates, and (iv) domain constraints such as aviation safety guidelines and mission-specific requirements, an LLM (GPT 3o is the selected model for experiments) proposes candidate Scallop rules encoding interpretable hazard logic (e.g., proximity to obstacles, containment of hazards, or exclusion zones). The generated rules are expressed directly as executable Scallop code operating over PSSG predicates.

The human-in-the-loop workflow. Figure 3 illustrates the human-in-the-loop offline construction and refinement of the symbolic reasoning engine from two complementary perspectives: the *system perception*, represented by nodes with a *green background*, and the *user interaction*, represented by nodes with a *yellow background*. System components operate automatically to construct, execute, and explain the reasoning engine, while user-facing components expose interpretable intermediate results and support targeted feedback. This separation enables domain experts to participate in the refinement process through intuitive visual inspection and high-level feedback, without requiring knowledge of symbolic programming, predicate logic, or rule execution semantics.

From the system perspective, the workflow begins with automated processing of raw aerial images. Semantic objects, attributes, and spatial relations are extracted and assembled into an explicit world model represented as *Scene Graph Components*, encoding the system's taxonomy of objects, attributes, and relations. Based on a task-specific initial prompt and the human-validated scene graph components produced by the *Post-processor*, an LLM synthesizes a candidate symbolic reasoning engine expressed as executable Scallop rules via *LLM Agent Processing*. The resulting reasoning engine is executed on top of the explicit world model in a simulation environment (e.g., *AirSim*) at the *Reasoning Engine Processing* node to evaluate candidate landing zones. This execution produces two structured outputs: (i) an annotated image highlighting predicted safe and unsafe landing regions, and (ii) a rule-trigger trace log that records which rules contributed to each decision. To support human interpretability, the trace log is automatically summarized into concise, human-readable explanations by the *Log Translation* module.

From the user perspective, human involvement is limited to a small number of well-defined inspection and feedback steps. Domain experts-such as engineers working with a drone delivery company-interact with the system exclusively through the annotated images and summarized rule explanations. At the *Need Refinement* node, experts review the predicted landing sites together with a short list of top rules triggered by the reasoning engine (e.g., exclusion due to proximity to pools or large obstacles). Based on this information, the expert determines whether the current reasoning behavior is acceptable or requires refinement.

When refinement is required, the expert provides high-level feedback in natural language at the *Provide Feedback* node, describing

Table 2: Representative Scallop rule examples for the safety gate.

ID	Scallop rule (Datalog style)	Intuition
R1	`landable_area(x) :- (paved_area(x) ∨ dirt(x) ∨ grass(x)).`	Paved, dirt, and grass are candidate landing surfaces.
R2	`human_related(y) :- (person(y) ∨ dog(y) ∨ bicycle(y) ∨ car(y)).`	Group human adjacent hazards.
R3	`hazard(x) :- landable_area(x), water(y), near_to(x, y).`	Water nearby is risky.
R4	`hazard(x) :- landable_area(x), tree(y), near_to(x, y).`	Large trees near touchdown are risky.
R5	`hazard(x) :- landable_area(x), pool(y), adjacent_to(x, y).`	Pools adjacent to a candidate are unsafe.
R6	`hazard(x) :- landable_area(x), rocks(y), contain(x, y), is_large_object(y).`	Large rocks in zone are unsafe.
R7	`hazard(x) :- landable_area(x), vegetation(y), contain(x, y), is_large_object(y).`	Dense vegetation in zone is unsafe.
R8	`hazard(x) :- landable_area(x), obstacle(y), contain(x, y), is_large_object(y).`	Generic large obstacle in zone is unsafe.
R9	`hazard(x) :- paved_area(x), car(y), contain(x, y).`	Vehicles occupying a paved zone are unsafe.
R10	`hazard(x) :- paved_area(x), human_related(y), contain(x, y).`	People, dogs, bicycles, cars in zone are unsafe.
R11	`hazard(x) :- landable_area(x), building(y), adjacent_to(x, y).`	Building adjacent to zone is risky.
R12	`hazard(x) :- landable_area(x), (area_too_small(x)∨ rough_surface(x)).`	Insufficient area or uneven surface.
R13	`safe(x) :- landable_area(x), not hazard(x).`	Safe if landable and no hazard fires.

observed issues or missing constraints. For example, an expert may note that regions near small obstacles are incorrectly marked as safe, or that landing zones should maintain larger safety margins or avoid overflight. Crucially, the expert is not required to specify rules, predicates, or logical conditions; feedback is expressed purely in domain-relevant terms. This feedback is processed by the *Prompt Rewriting* module, which generates a refined prompt for the LLM to synthesize an updated reasoning engine. The refined engine then enters the next refinement cycle, where it is re-executed on the same pre-validated world model in the simulation environment to produce updated landing predictions and human-readable rule explanations. The loop continues until the expert determines that no further feedback is required.

3.2.2 Execution on the world model. At runtime, the validated rule pack is executed directly over the online probabilistic semantic scene graph (PSSG). The reasoning engine operates entirely on the explicit world model-comprising objects, attributes, and spatial relations-rather than on raw pixels or latent features. This design ensures that hazard and safety assessments are grounded in inspectable symbolic representations.

Scallop evaluates the rule pack as a probabilistic first-order logic program and answers queries such as hazard(i) and safe(i) for each candidate region r_i. For each query, Scallop enumerates the top-k highest-weight proofs and aggregates them to compute calibrated hazard and safety scores. Provenance traces record which rules and world-model facts contributed to each proof, enabling concise explanations and supporting debugging and auditing. A region is inferred as safe if its estimated safety score exceeds a mission-specific threshold.

Example. As a concrete example, a region may be classified as hazardous if it is *near-to* an obstacle with sufficiently high confidence:

$$\text{hazard}(i) \;:-\; \text{near\_to}(i, j)[p_1],\ \text{obstacle}(j)[p_2],\ p_1 \otimes p_2 > \tau.$$

Here, near_to(i, j) and obstacle(j) are probabilistic predicates derived from the PSSG, and $\otimes$ denotes a confidence-composition operator. The threshold τ is *not chosen arbitrarily*; it is calibrated offline through simulation-based validation and human-in-the-loop refinement to reflect domain safety requirements rather than ad hoc tuning. Because τ is encoded as part of an explicit symbolic rule, it can be inspected, justified, and revised independently of the perception stack.

By synthesizing the symbolic reasoning engine offline and executing it directly over the PSSG online, NeuroSymLand cleanly separates perception from reasoning while enabling interpretable, debuggable, and mission-adaptable hazard assessment for landing site selection.

3.3 Multi-Frame Validation and Mission-Specific Ranking

Multi-frame validation. To reduce false positives caused by transient segmentation noise, brief occlusions, or short-lived perception

errors, candidate regions are validated across a short temporal window of recent frames. Let $\mathcal{W}_T = \{t_0 - T + 1, \ldots, t_0\}$ denote a window of T consecutive frames ending at time t_0, and let $v^{(t)}$ denote the instance of region v at time t.

A candidate region passes multi-frame validation if it satisfies two conditions over the entire window: (i) it is never inferred as hazardous, and (ii) its geometric properties remain stable. Formally, we define

$$\mathrm{Pass}_T(v) \equiv \bigwedge_{t \in \mathcal{W}_T} \neg\,\mathrm{hazard}(v^{(t)}) \wedge \neg\,\mathrm{Jitter}(v^{(\mathcal{W}_T)}),$$

where $\mathrm{hazard}(v^{(t)})$ is the hazard predicate inferred by the rule-based reasoning engine at time t, and $\mathrm{Jitter}(\cdot)$ is a binary predicate that returns `true` if significant geometric instability (e.g., abrupt changes in centroid or area) is detected across the window. No additional threshold or hyperparameter is introduced for jitter; a region either exhibits jitter or it does not. We denote by $\mathbb{I}_T(v) = \mathbf{1}\{\mathrm{Pass}_T(v)\}$ whether region v satisfies multi-frame validation.

Mission-specific ranking. Candidate regions that pass multi-frame validation are considered admissible for landing. Final selection is performed by ranking validated candidates using a mission-specific utility function that encodes task priorities. For each mission m, a set of normalized features $\tilde{b}_{m,k}(v) \in [0, 1]$ (e.g., landing area, distance to target, estimated energy cost) is computed, together with nonnegative weights $\omega_{m,k}$ reflecting the relative importance of each feature. In particular, we instantiate distinct weight profiles for three mission modes: for *rescue landing*, proximity to the target person is prioritized by assigning a high weight to the distance-to-person feature; for *emergency landing*, immediate maneuver economy is emphasized by heavily weighting a landing-cost term such as distance to the current image center (or UAV projection); and for *safe landing* (default), intermediate weights balance safety margin, landing area, and maneuver cost.

The mission-conditioned score of a candidate region v is defined as

$$C_m(v) = \mathbb{I}_T(v) \sum_k \omega_{m,k}\, \tilde{b}_{m,k}(v), \qquad v^\star = \arg\max_v C_m(v).$$

Candidates that fail multi-frame validation receive zero score and are excluded from ranking, while validated regions are ordered according to mission-aligned utility.

4 Experiments

4.1 Research Questions

We investigate the following research questions (RQs) to assess the proposed neuro-symbolic landing framework, NeuroSymLand:

RQ1 *Effectiveness of explicit world modeling and reasoning.* To what extent does NeuroSymLand improve safe landing site detection in software-in-the-loop (SIL) simulations compared with learning-based and hybrid state-of-the-art baselines? To isolate the contribution of the symbolic reasoning engine, we further introduce an ablation variant, NeuroSymLand-DetFOL, which replaces the human-in-the-loop–constructed Scallop reasoning engine with a set of manually specified deterministic first-order logic rules, enabling direct evaluation of the benefits brought by learned symbolic reasoning over the same explicit world model.

RQ2 *Practical deployability and efficiency on edge hardware.* Can NeuroSymLand be executed efficiently on resource-constrained edge platforms under hardware-in-the-loop (HIL) evaluation, and how does its runtime performance compare with lightweight learning-based baselines in terms of inference latency and system resource usage?

RQ3 *Interpretability and reasoning quality.* Even when comparable landing success rates and inference efficiency are achieved, how do NeuroSymLand and competing baselines differ in terms of reasoning transparency, human interpretability, and alignment with domain-inspired safety logic? Through a detailed qualitative case study, we examine how explicit world modeling and white-box symbolic reasoning support human understanding compared with opaque learning-based approaches and LLM/VLM based (implicit) reasoning approaches.

To address the **RQs**, we evaluate the proposed landing-site selection framework through three complementary study types:

- **Software-in-the-Loop (SIL) evaluation (RQ1).** We conduct controlled simulation experiments on a fixed set of **72 simulated landing scenarios** under default environmental conditions. All methods are executed multiple times per scenario to ensure stable and fair comparison.
- **Hardware-in-the-Loop (HIL) evaluation (RQ2).** We assess computational feasibility on the target edge platform (Jetson Orin Nano) using recorded simulation inputs. The HIL study measures end-to-end runtime performance and system resource usage, and compares latency against baselines deployable on the same platform (SafeUAV and SegOpticalFlow).
- **Qualitative case studies (RQ3).** We perform qualitative comparisons across *all evaluated baselines* on representative scenarios drawn from the 72-scenario set. Case studies cover three mission contexts-*Emergency Landing*, *Rescue Landing*, and *Safe Landing*-and focus on interpretability, and reasoning transparency.

4.2 RQ1: Effectiveness

Accordingly, we evaluate landing-site assessment (LSA) performance using two metrics: (i) the number of successful landings, which captures task feasibility, and (ii) a quality measure computed on successful predictions to characterize safety margin.

Successful Landings (Succ↑). Because markerless LSA provides no external ground-truth touchdown annotations, we first assess whether a predicted landing location results in a safe and feasible touchdown under our evaluation protocol. We report the total number of successful landings (and the corresponding success rate when normalized by the number of trials). This metric reflects end-to-end *decision reliability*: a method that predicts nominally safe regions but frequently results in unsafe outcomes under evaluation is unsuitable for safety-critical UAV operations.

Quality of Successful Predictions. For trials deemed successful, we further quantify *how safe* the predicted touchdown is using an interpretable geometric metric. Let $\hat{\mathbf{p}} \in \mathbb{R}^2$ denote the predicted touchdown point, O the set of obstacle boundary points (e.g., fences, building edges, pool rims, trees), and $\|\cdot\|_2$ the Euclidean norm. We quantify safety margin using the *Minimum Obstacle Distance (MOD↑)*, defined as

$$\text{MOD} = \min_{\mathbf{o} \in O} \left\| \hat{\mathbf{p}} - \mathbf{o} \right\|_2,$$

where larger values indicate safer buffers from surrounding obstacles.

Experiment Setup. We conduct evaluations in *AirSim* [54] using **72 distinct landing scenarios** that represent common UAV operating environments, including *city streets*, *suburban areas*, *industrial yards*, *parking lots*, *parks and grass fields*, and *construction sites*. All experiments are performed under **default environmental conditions** (i.e., without varying weather, wind, or time of day) to ensure controlled and fair comparisons across methods. For each method, we report the number of **successful landings (Succ)** and summarize the quality of successful predictions using the **Minimum Obstacle Distance (MOD)**, where larger values indicate safer landing margins. To capture both typical and conservative performance, we report the **median** and the **20th percentile (P20)** of MOD across scenarios, aggregated over five runs per scenario. Because the experimental setting is fixed, performance variability is dominated by scenario diversity, while variation across repeated runs within the same scenario is minimal.

Baselines. We do not directly benchmark against prior markerless landing pipelines [43, 52, 55] that rely on sensing or infrastructure assumptions outside our setting, such as active depth sensors, LiDAR, or full SLAM-based world reconstruction. These approaches entangle landing-site assessment performance with sensing coverage, persistent mapping, and long-horizon observability, making it difficult to isolate improvements attributable specifically to safe landing assessment and reasoning.

Instead, we evaluate against a set of lightweight baselines that operate under the same monocular perception setting and adopt a comparable candidate landing representation. This ensures that observed performance differences primarily reflect variations in safe landing assessment (SLA) and reasoning behavior, rather than differences in sensing modality or mapping support. We further include two recent and representative segmentation-oriented markerless landing systems, **SafeUAV**[41] and **PEACE**[12], which predict safe landing regions as pixel-level mask maps from monocular RGB images.

In addition, we include an explicit **ablation study**, **NeuroSymLand-detfol (Ablation)**, in **RQ1** to evaluate the contribution of neuro-symbolic reasoning beyond deterministic logic under an identical explicit world model (probabilistic spatial scene graph). All baselines operate on the same candidate landing representation and, where applicable, share the same perception backbone as NeuroSymLand.

- **SegOpticalFlow** [26, 51]: a perception-only baseline that scores candidate landing sites using multi-frame optical flow estimates. It shares the same perception backbone as NeuroSymLand and employs the same mission-specific ranking selector, isolating the effect of reasoning from perception.
- **NeuroSymLand-detfol (Ablation)** [31, 50]: a deterministic first-order logic (FOL) variant of NeuroSymLand that uses the same explicit world model, rule structure, and candidate site representation, and shares the same perception backbone. Unlike NeuroSymLand, which synthesizes executable Scallop programs through an offline neuro-symbolic pipeline, NeuroSymLand-detfol evaluates hand-crafted FOL predicates deterministically at runtime. This ablation isolates the benefit of neuro-symbolic synthesis-such as probabilistic rule bindings and learned confidence composition-from the logical structure itself.
- **LLMExplain** [2]: a local vision–language model baseline (Phi-3.5 Vision [1]) prompted with the scene image and encoded safety rules. The model selects among the same candidate landing sites and outputs a concise textual rationale. This baseline evaluates whether end-to-end VLM-based decision making remains reliable under mission-critical constraints, and whether explicit logical guardrails improve decision consistency and safety compliance.
- **SafeUAV** [41]: a lightweight embeddable convolutional network that estimates depth and segments monocular RGB images into safe landing and obstacle regions. Its output is a pixel-level safe-region mask rather than a single landing point.
- **PEACE** [12]: a prompt-adaptation framework for open-vocabulary segmentation that dynamically refines prompts to identify safe landing regions under distribution shifts. It performs dual segmentation of safe and unsafe zones and refines candidate regions by excluding unsafe areas. Similar to SafeUAV, its output is a safe-region mask rather than a single landing location.

Mask-to-point conversion for evaluation. Unlike NeuroSymLand and other point-based baselines that output an explicit touchdown point, the two recent segmentation-oriented baselines, **SafeUAV** and **PEACE**, predict pixel-level binary masks indicating safe landing regions. To enable consistent point-based evaluation with **Succ** and **MOD**, we convert these mask outputs into a proxy touchdown location by computing the centroid of the largest connected component in the predicted safe mask. If the predicted safe mask is empty, the method is treated as producing no valid landing proposal for that trial; such cases are counted as unsuccessful, and MOD is not computed. This conversion allows us to include these recent, representative segmentation-based approaches in a unified evaluation protocol while preserving their original output semantics and enabling fair comparison with methods that produce explicit touchdown points.

Result Analysis. Table 3 summarizes the quantitative results for **RQ1**. We use **Succ** as the primary metric because it directly reflects the reliability of landing-site safety assessment in the markerless setting. In this context, a method may either (i) abstain from making a decision when no candidate is deemed safe, or (ii) produce a

(a) Distinctive success case (RGB + predictions).

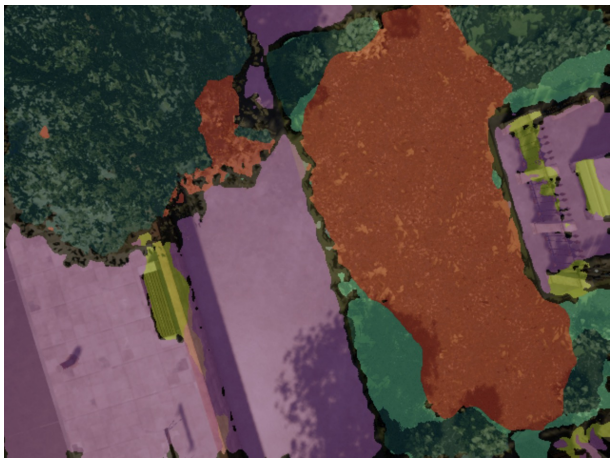

(b) Corresponding semantic segmentation.

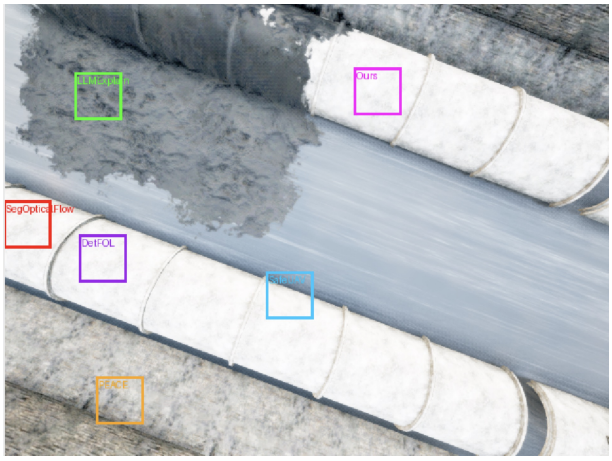

(c) Perception-limited case (RGB + predictions).

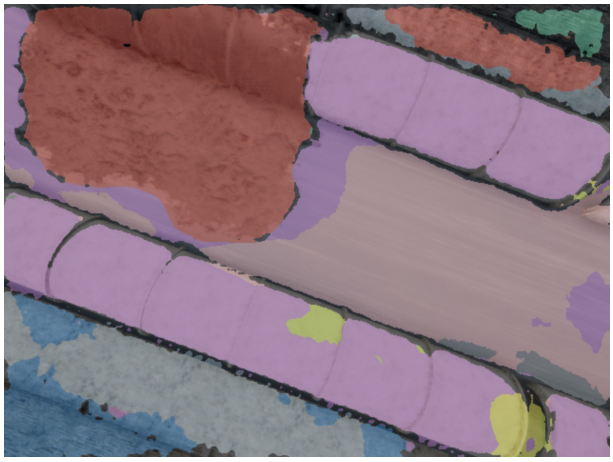

(d) Corresponding semantic segmentation.

Figure 4: Qualitative examples of landing-site safety assessment in AirSim. Each row shows one representative scenario. Left: RGB images overlaid with predicted landing-site locations from different methods, where colored markers indicate the selected candidate site for each method. If a marker is absent, the corresponding method does not produce any candidate decision for that scenario. Right: semantic segmentation results used to construct the explicit world model, with colors indicating different semantic classes. The top row illustrates a scenario where only a subset of methods produce a safe landing-site decision. The bottom row illustrates a perception-limited scenario in which none of the evaluated methods identify a safe landing-site candidate.

decision that does not fall within the human-annotated safe landing zone. Accordingly, we report **Succ** as **Count/Dec.**, where **Dec.** denotes the number of scenarios in which the method produces at least one candidate decision, and **Count** denotes the number of scenarios in which the predicted explicit touchdown point lies within the annotated safe zone. The gap between these two quantities is informative: a low **Dec.** indicates conservative abstention, whereas a large gap between **Dec.** and **Count** indicates permissive decision making that frequently violates safety constraints.

Across all baselines, NeuroSymLand achieves the highest success count (**61/72**), followed by the ablation variant NeuroSymLand-detfol (**58/71**) and the strongest state-of-the-art baseline, **PEACE** (**57/72**), a recent IROS 2025 VLM-based method. Although the absolute margin in success count may appear modest, it is important to interpret these results in light of the difficulty of the remaining scenarios. In many challenging cases, failures are not due to the absence of any flat region, but to subtle interactions among spatial layout, semantic context, and safety constraints-precisely the situations where implicit reasoning underneath modern foundation/VLM models through end-to-end learning struggles.

The comparison between NeuroSymLand-detfol and PEACE highlights the benefit of an explicit world model. Even when both operate over the same perception backbone and candidate representation, the explicit probabilistic spatial scene graph enables

Table 3: Landing-site safety assessment on the AirSim test set. Succ. is reported as Count/Dec., where Dec. denotes the number of scenarios in which the method produces at least one landing-site safety assessment decision (i.e., identifies one or more candidate sites), and Count denotes the number of scenarios in which the predicted explicit touchdown point lies within the human-annotated safe landing zone. MOD is reported in pixels as median / 20th percentile (P20), where larger values indicate larger safety margins to surrounding obstacles.

Method	Succ.↑ Count / Dec.	MOD (px)↑ median / P20
NeuroSymLand	**61/72**	119.64 / 28.0
SegOpticalFlow	53/63	**159.40 / 51.19**
PEACE	57/72	84.38 / 42.43
SafeUAV	47/72	74.48 / 18.36
LLMExplain	37/72	52.00 / 13.0
NeuroSymLand-detfol (Ablation)	58/71	104.61 / 41.4

NeuroSymLand-detfol to identify one additional safe scenario that the VLM-based approach misses. More importantly, the full NeuroSymLand improves upon NeuroSymLand-detfol by a further **four scenarios**, demonstrating that the gain does not stem solely from symbolic structure, but from the neuro-symbolic reasoning engine itself. Unlike hand-crafted deterministic FOL rules, the synthesized Scallop programs support probabilistic bindings and soft rule composition, and encode domain knowledge distilled through the human-in-the-loop construction and refinement process. This enables NeuroSymLand to better handle edge cases where safety depends on the joint satisfaction of multiple weak cues rather than a single hard constraint.

We emphasize that the remaining 11 scenarios missed by NeuroSymLand are not failures of reasoning alone. In all such cases, NeuroSymLand still produces a decision, but the decision is constrained by errors inherited from the perception foundation model. As shown in the qualitative analysis below, these perception-limited scenarios are challenging for all evaluated methods, including VLM-based and segmentation-based approaches.

Overall, while the numerical improvement in **Succ** over strong baselines such as PEACE seems incremental, the results indicate a meaningful shift in capability. Explicit world modeling enables systematic reasoning about safety constraints, and neuro-symbolic rule synthesis further extends this capability beyond what deterministic logic or implicit VLM reasoning can achieve. The qualitative differences observed in edge cases carefully analyzed below, rather than raw success counts alone, therefore form the core contribution of NeuroSymLand.

It is also important to interpret MOD jointly with decision coverage. Although **SegOpticalFlow** attains the highest MOD, this outcome reflects a highly conservative strategy that frequently abstains from producing any landing decision in challenging scenes. It produces landing decisions in 63 out of 72 landing scenarios, reflecting the most conservative decision strategy among all methods. As a result, MOD for SegOpticalFlow is computed only on a small subset of easy cases with large, unobstructed free space, which naturally inflates clearance statistics.

In contrast, NeuroSymLand produces a landing decision in all scenarios and achieves the highest overall success count. Its MOD therefore reflects safety margins under a much broader and more challenging set of conditions, including cluttered and ambiguous environments where conservative baselines often abstain. This behavior highlights an inherent trade-off between selective high-clearance outcomes and actionable, interpretable safety assessment, with NeuroSymLand favoring systematic reasoning and coverage without sacrificing meaningful obstacle clearance.

Case studies. Figure 4 presents two representative scenarios selected from the 72-scenario set to illustrate (i) where NeuroSymLand 's explicit world modeling and reasoning provide qualitatively different behavior from strong implicit baselines, and (ii) a perception-limited regime in which semantic errors constrain all evaluated methods.

Case A: Qualitatively distinctive behavior under ambiguous semantics (top row). In this scenario, the segmentation foundation model produces non-trivial noise (e.g., local regions of grass/bare ground partially mislabeled as *water*), which fragments or corrupts the apparent landable area. Despite this, NeuroSymLand still produces a candidate that falls within the human-annotated safe landing zone by reasoning over the probabilistic spatial scene graph (PSSG) and composing multiple safety constraints over explicit objects, attributes, and relations, rather than committing to a single hard mask interpretation. This capability is qualitatively different from baselines whose decision making is dominated by implicit or purely perception-driven criteria: conservative methods may abstain when the predicted safe region becomes uncertain or fragmented (reducing **Dec.**), while end-to-end VLM/VLM-style baselines can be sensitive to ambiguous visual cues and may produce decisions that are less consistently grounded in explicit spatial constraints. Segmentation-only approaches may also yield candidates with smaller obstacle clearance in this case, as their outputs provide limited structured provenance beyond the predicted mask.

Case B: Perception-limited regime shared by all methods (bottom row). The second scenario exemplifies a regime where the semantic abstraction itself is incorrect (e.g., cylindrical pipes mislabeled as *landable surface* and surrounding concrete mislabeled as *water*), distorting the inferred free space and obstacle layout. Under such corrupted semantics, none of the evaluated methods identify a safe landing-site candidate that matches the human-annotated safe zone, including NeuroSymLand. Importantly, this outcome should not be interpreted as a failure of the symbolic reasoning logic alone; rather, it reflects a common limitation of semantic-driven landing-site assessment pipelines: the reasoning layer (explicit or implicit) is bounded by the reliability of the perceptual inputs it consumes. These case studies provide context for the quantitative results in Table 3. First, the remaining 11 scenarios missed by NeuroSymLand are not failures of reasoning alone: NeuroSymLand still produces a decision in every scenario, but in the most challenging cases

the decision is constrained by errors inherited from the perception foundation model-a limitation that also affects VLM-based and segmentation-based baselines. Second, while the improvement in **Succ** over strong baselines such as PEACE is numerically incremental, it corresponds to meaningful differences in edge cases where safety depends on joint satisfaction of multiple weak cues and constraints. Finally, the comparison between NeuroSymLand and NeuroSymLand-detfol highlights that human-in-the-loop synthesis of executable Scallop programs can provide additional robustness beyond hand-coded deterministic rules, through probabilistic bindings and soft composition over the same explicit world model. Collectively, these observations motivate tighter, reciprocal neuro-symbolic integration as a future direction: when reasoning outcomes are inconsistent with safety expectations (e.g., repeated low-margin or unsafe candidates), this signal can guide targeted refinement of the perception foundation model and the world-model extraction process, improving reliability in perception-limited regimes.

4.3 RQ2: Efficiency

To quantify the end-to-end responsiveness and computational efficiency of NeuroSymLand under realistic input–output conditions, we conduct a hardware-in-the-loop (HIL) evaluation on the target edge platform.

Setup. All HIL experiments are conducted on a Jetson Orin Nano with 8 GB RAM, running Ubuntu 22.04 with CUDA 12.6 and ONNX Runtime 1.19. The perception stack employs *SegFormer-B0-INT8* for semantic segmentation, and the system interfaces with the *PX4 Autopilot* via the *MAVROS/ROS 2 Humble* bridge at a fixed 30 Hz update rate. All experiments are executed in *AirSim* [54] under **default simulation settings**.

For efficiency evaluation, we execute 100 trials with randomized initial poses and headings sampled from a representative simulation map. This setting captures runtime variability while keeping environmental and task conditions controlled. For each trial, we measure end-to-end inference latency-from image acquisition to landing-site safety assessment output-as well as stage-wise execution time, including semantic segmentation and post-processing, probabilistic spatial scene graph (PSSG) construction, symbolic reasoning, and mission-specific ranking (MSR). We additionally record system-level metrics, including CPU and GPU utilization, memory footprint, power consumption, and operating temperature.

To contextualize efficiency and latency, we compare NeuroSymLand against two lightweight baselines: **SegOpticalFlow** and **SafeUAV**. These baselines represent established industry-style practices for markerless landing-site safety assessment and are sufficiently lightweight to be deployed on the same edge platform and execution stack. SegOpticalFlow reflects a perception-driven, motion-based design commonly used in embedded UAV systems, while SafeUAV represents a compact learning-based approach tailored for monocular RGB input.

We exclude other baselines from RQ2 because they rely on substantially heavier foundation-model or VLM backbones with compute and memory requirements that exceed the target deployment budget of embedded UAV platforms. In particular, **PEACE** and **LLMExplain** cannot be executed on the Jetson Nano under our deployment configuration and consistently trigger out-of-memory (OOM) failures during inference. Including such methods would conflate algorithmic efficiency with fundamentally different system assumptions, making the comparison uninformative for practical edge deployment.

Results analysis. All results are reported as **median ± standard deviation** over 100 repeated HIL trials, unless otherwise noted.

Stage-wise latency breakdown. Table 4b reports the stage-wise latency of NeuroSymLand. Summing the median latencies across all stages yields an end-to-end median inference time of approximately 1,043.3 ms per frame, corresponding to about 0.96 FPS on the Jetson Orin Nano under our deployment stack.

The dominant runtime cost arises from **PSSG construction** (557.1 ± 72.0 ms), which accounts for approximately 53% of the total median latency. This stage includes probabilistic scene graph assembly and relational encoding, which are inherently more expensive than pure feed-forward perception. The second largest contributor is **perception and post-processing** (424.4 ± 30.7 ms, ∼ 41%), reflecting the cost of semantic segmentation and associated filtering.

In contrast, the **symbolic reasoning engine** is lightweight, requiring only 20.0±5.6 ms (about 2% of total latency). This confirms that explicit symbolic reasoning introduces negligible overhead relative to perception and world-model construction. The **mission-specific ranking (MSR)** stage further contributes a small and stable cost of 41.8 ± 3.6 ms (∼ 4%). Overall, the latency breakdown demonstrates that the computational bottleneck lies in perception and world modeling rather than in symbolic inference.

System-level resource usage. System utilization statistics are summarized in Table 4c. On the Jetson Nano, NeuroSymLand consumes a median of 76.87% CPU and 52% GPU utilization, with a memory footprint of 5.6 GB, power draw of 1.23 W, and operating temperature of 47.91°C. These values indicate stable operation within the thermal and power envelope of the target platform.

Compared with lightweight baselines, **SegOpticalFlow** exhibits lower CPU utilization (59.82%) with similar GPU utilization (56%), and slightly reduced memory usage (5.3 GB), power consumption (1.07 W), and temperature (45.20°C), reflecting its purely perception-driven design. **SafeUAV** shows a median of 49.1% CPU and 55% GPU utilization, with 5.2 GB memory usage, 1.2 W power draw, and 49.82°C operating temperature. Overall, the additional overhead introduced by explicit world modeling and symbolic reasoning remains modest and does not compromise system stability on embedded hardware.

End-to-end latency comparison. To contextualize the absolute latency of NeuroSymLand, we compare end-to-end inference throughput with SegOpticalFlow and SafeUAV (Table 4a). NeuroSymLand achieves a median throughput of 0.95 FPS, corresponding to 1051.4 ms per frame. In comparison, **SegOpticalFlow** attains 1.16 FPS (861 ms), while **SafeUAV** achieves 8.00 FPS (125 ms).

Although NeuroSymLand incurs higher end-to-end latency due to explicit world model construction and mission-specific scoring, its refresh rate remains within practical limits for pre-landing safety assessment, where decision updates on the order of 0.5–1 s per frame are often sufficient. Notably, **SafeUAV** achieves lower

Table 4: Hardware-in-the-Loop (HIL) evaluation on Jetson Nano (median over 100 trials).

(a) End-to-end inference latency (ms)

Method	End-to-end latency (ms)
NeuroSymLand (ours)	med = 1051.4 σ = 86.7
SegOpticalFlow	med = 861 σ = 2.65
SafeUAV	med = 125 σ = 2.4

(b) Stage-wise latency breakdown of NeuroSymLand

Stage	Percep. + Post.	PSSG	Reasoning	MSR
Latency (ms)	med = 424.4 σ = 30.7	med = 557.1 σ = 72.0	med = 20.0 σ = 5.6	med = 41.8 σ = 3.6

(c) System resource usage on Jetson Nano

Method	CPU (%)	GPU (%)	Mem (GB)	Power (W)	Temp (°C)
NeuroSymLand (ours)	76.87	52	5.6	1.23	47.91
SegOpticalFlow	59.82	56	5.3	1.07	45.20
SafeUAV	49.1	55	5.2	1.2	49.82

latency primarily because it adopts a lightweight U-Net–style segmentation backbone, whereas our perception module employs a Transformer-based backbone that is more compute-intensive but yields richer semantic representations for explicit world modeling and downstream reasoning. However, this efficiency comes with clear performance trade-offs. As shown in Table 3, **SafeUAV** identifies suitable landing sites in only **47 out of 72 scenarios**, the second lowest success count among all evaluated methods, and attains one of the smallest MOD values, indicating consistently reduced clearance to nearby obstacles and therefore smaller safety buffers around the selected landing sites. These results suggest that while SafeUAV is sufficiently lightweight for real-time execution, its perception-only design limits reliability and safety margins in cluttered or ambiguous environments compared to approaches that explicitly reason over spatial structure and safety constraints.

4.4 RQ3: Interpretability and reasoning quality

Evaluation setup. RQ3 focuses on qualitative assessment of reasoning transparency, human interpretability, and alignment with domain-inspired safety logic. Unlike RQ1 and RQ2, the objective here is not to compare detection accuracy or computational efficiency, but to examine how different approaches support human understanding of *why* a landing-site safety decision is made and how such decisions adapt to task-dependent priorities.

We consider all baselines applicable to qualitative inspection under a monocular, markerless landing-site safety assessment setting, including **SafeUAV**, **SegOpticalFlow**, **PEACE**, and **LLMExplain**, together with NeuroSymLand.

Existing baselines primarily assess landing suitability using fixed geometric or appearance-based cues. In particular, **SafeUAV** and **SegOpticalFlow** identify regions that satisfy generic safety constraints (e.g., obstacle clearance or motion consistency), without encoding task-dependent preferences. **PEACE** produces segmentation-based safe-region masks through prompt adaptation but does not expose an explicit reasoning structure, while **LLMExplain** relies on implicit reasoning within a vision–language model, producing natural-language explanations that are not explicitly grounded in symbolic or spatial constraints.

Mission-conditioned reasoning. In contrast, NeuroSymLand introduces an explicit mission-specific ranking mechanism that operates over a shared set of landing-site candidates derived from the same world model. Task-dependent priorities are captured by dynamically adjusting the weights of symbolic predicates, while keeping the underlying reasoning logic unchanged. We consider three mission contexts that reflect common UAV operational needs:

- **Emergency:** prioritizes minimal distance to a predefined mission center, favoring rapid and nearby touchdowns under time-critical conditions.
- **Rescue:** prioritizes minimal distance to a designated target (e.g., a waypoint or person of interest), emphasizing proximity to the rescue objective.
- **Safe-Landing:** prioritizes safety margins by penalizing proximity to hazards (e.g., roads, buildings, water, crowds) and unfavorable surface conditions (e.g., slope, roughness), encouraging conservative touchdown locations.

These mission contexts share the same perception pipeline and world model, but differ in the mission-specific rule program and the weighting used for candidate scoring and ranking.

Case-study protocol. For the qualitative case study, all methods are applied to identical visual inputs drawn from a selected scenario in the 72-map test set (the skateboard park). Baselines are evaluated in their original form, without modification or added explanations. Methods that output region masks are visualized using their predicted safe areas, while methods that output explicit touchdown points are visualized by their selected candidate locations.

For NeuroSymLand, we present the original image alongside three mission-specific outputs corresponding to *Emergency*, *Rescue*, and *Safe-Landing* contexts. The perception pipeline and the resulting world model are held fixed across all three outputs. Mission adaptation is achieved by switching the mission-specific rule set and adjusting the mission-conditioned weights in the candidate ranking stage, while operating over the same set of sampled landing candidates.

Results. Both **SafeUAV** and **PEACE** assess landing suitability primarily through dense region-level predictions. As shown in Fig. 5, both methods label large contiguous paved areas as safe, producing broad green masks that cover most of the visually homogeneous surface. However, these outputs do not explicitly differentiate candidates based on proximity to nearby pedestrians or small obstacles visible in the scene. As a result, multiple candidate locations with varying stand-off distances to hazards are treated equivalently in the final visualization.

LLMExplain produces a single landing recommendation accompanied by a natural-language rationale. Although the explanation is human-readable, it attributes the decision to high-level descriptors such as an "open grassy region", which does not accurately reflect the underlying scene geometry. In practice, the selected landing area is only relatively safe and does not correspond to a clearly open or obstacle-free region. Because the decision is not grounded in explicit, verifiable spatial constraints (e.g., quantified

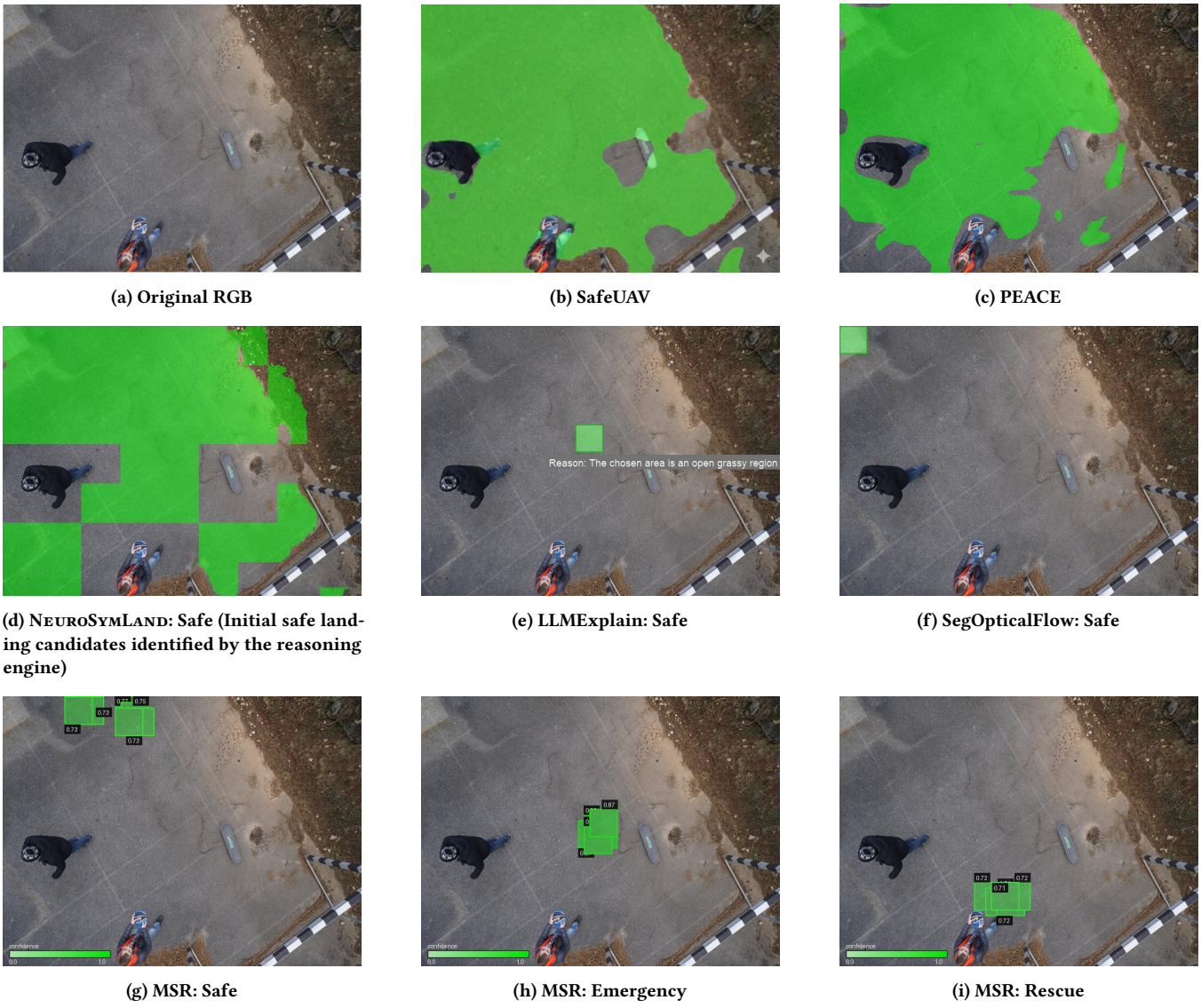

(a) Original RGB (b) SafeUAV (c) PEACE

(d) NeuroSymLand: Safe (Initial safe landing candidates identified by the reasoning engine) (e) LLMExplain: Safe (f) SegOpticalFlow: Safe

(g) MSR: Safe (h) MSR: Emergency (i) MSR: Rescue

Figure 5: Qualitative case study on an AirSim test scene. (a) Original RGB image. (b–c) Dense safe-region predictions produced by learning-based baselines (SafeUAV and PEACE). (d) Safe-region result from NeuroSymLand after symbolic safety-rule reasoning under the default mission. (e–f) Safe-region outputs from LLM-based (LLMExplain) and motion-based (SegOpticalFlow) baselines. (g–i) Mission-conditioned landing-site selection by NeuroSymLand, showing the top-ranked (5) candidates under safe, emergency, and rescue missions, respectively. Unlike baselines that predict static safe regions, NeuroSymLand integrates symbolic rules with mission context to produce interpretable, task-adaptive landing decisions.

distances to nearby people or obstacles), the rationale cannot be reconciled with the actual layout of the environment. More fundamentally, the explanation is generated post hoc from an implicit model whose internal weight matrix is not amenable to systematic testing or verification. As a result, the reasoning process lacks transparency and cannot be inspected, validated, or aligned with human-defined safety logic, limiting its suitability for safety-critical decision making. **SegOpticalFlow** outputs a single landing point near the upper-right corner of the scene, without exposing intermediate safety scores or alternative candidates. As a result, the rationale for preferring this location over other geometrically feasible regions remains implicit and cannot be adapted to different mission priorities.

In contrast, NeuroSymLand produces an explicit neuro-symbolic safety assessment under the default **Safe-Landing** context. Although the resulting safe region in Fig. 5(d) may appear visually similar to the outputs of **SafeUAV** and **PEACE**, the underlying decision mechanism is fundamentally different and fully interpretable. In segmentation-based approaches, low-confidence or misclassified *person* regions from the perception foundation model can cause

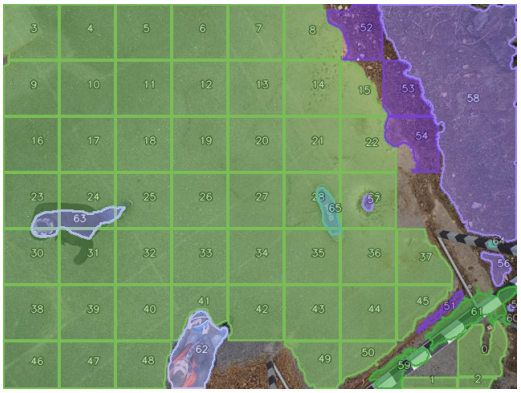

Figure 6: Semantic node distribution (Ours). Calibrated segmentation is overlaid on the RGB frame; colors indicate classes (e.g., paved, vegetation, person, obstacle). The white grid is the spatial index used for candidate sampling, with zone IDs shown at centers.

Table 5: Rule-level attribution from Scallop provenance for the case study run. For each safety rule r_*, we report the mean provenance proof weight (p) over triggered frames and the trigger count.

Rule r_*	p	Count
r_hazard_near_person	0.89	9
r_hazard_near_obstacle	0.91	4
r_hazard_near_wall	0.97	4
r_hazard_cont_veg	0.99	1
r_hazard_adj_pool	0.00	0
r_hazard_near_tree	0.00	0
r_hazard_near_car	0.00	0
r_hazard_near_rocks	0.00	0
r_hazard_near_bicycle	0.00	0
r_hazard_near_dog	0.00	0
r_hazard_adj_fence	0.00	0

Notes. Values are derived from Scallop's provenance under `difftopkproofsdebug`. For a triggered rule instance, the proof weight is computed as the product of the weights of its supporting facts (node semantic confidences and relation probabilities). The reported p is the *mean* proof weight across all frames in which the rule is triggered, and *Count* is the number of triggered frames. These statistics indicate which safety constraints most frequently and strongly drive the hazard assessment for the selected landing candidate(s).

areas close to real pedestrians to be incorrectly retained as safe, leading both the recent IROS 2025 method **PEACE** and the industry-grade **SafeUAV** to select landing sites that violate intended stand-off requirements.

By contrast, NeuroSymLand explicitly encodes *near-person* as a symbolic hazard through its reasoning rules. As illustrated in the mission-specific analysis below, multi-frame validation and mission-specific ranking—where safety is assigned the highest priority in the **Safe-Landing** setting—ensure that candidate sites with insufficient clearance to people are consistently rejected. As a result, NeuroSymLand selects landing regions that remain farther from the ground-truth pedestrian location, even when the underlying perception model exhibits uncertainty, yielding decisions that are not only safer but also transparent and explainable.

Under the **Emergency** context, the symbolic cost function shifts priority toward proximity to the mission center while still enforcing minimum safety constraints. Accordingly, NeuroSymLand selects a landing site near the scene center that preserves an adequate buffer from surrounding hazards.

Under the **Rescue** context, the cost function instead prioritizes proximity to a designated target (e.g., a waypoint or person of interest). The resulting landing site is adjacent to, but does not overlap with, the target footprint, satisfying non-intersection constraints while maintaining a workable safety margin. Across all three mission contexts, the perception pipeline, world model, and symbolic rule set remain unchanged; only the mission-conditioned weights differ, highlighting the role of explicit reasoning in adapting behavior without retraining.

Rule-level analysis and interpretability. Beyond visual differences, NeuroSymLand provides explicit traceability for its decisions. Rather than producing an opaque output as in end-to-end learning-based baselines, NeuroSymLand yields a *proof-carrying* landing assessment whose outcome can be traced to concrete symbolic rules and grounded facts.

Figure 6 shows the calibrated semantic segmentation overlaid with the evaluation grid, illustrating the set of landing candidates extracted from the image, including multiple zones located on paved surfaces.

An inspection of the aggregated Scallop provenance statistics (Table 5) reveals that the hazard assessment across all landing candidates in this scene is primarily driven by a small set of proximity-based safety rules. In particular, `r_hazard_near_person`, `r_hazard_near_obstacle`, and `r_hazard_near_wall` exhibit the highest trigger counts and mean proof weights, indicating that stand-off constraints with respect to people, obstacles, and nearby structures dominate the safety evaluation. A vegetation-related constraint (`r_hazard_cont_veg`) is activated only once, while all remaining hazard rules (e.g., pools, trees, vehicles, fences, rocks, bicycles, and animals) are not triggered in this scene.

At the symbolic level, the dominant proofs correspond to conjunctions of grounded facts of the form $\text{paved\_area}(x) \otimes \text{person}(y) \otimes \text{near\_to}(x, y)$, $\text{paved\_area}(x) \otimes \text{obstacle}(z) \otimes \text{near\_to}(x, z)$, and $\text{paved\_area}(x) \otimes \text{wall}(w) \otimes \text{near\_to}(x, w)$, where (x, y, z, w) range over landing candidates and nearby scene objects. These proof patterns capture the recurring safety violations observed across the candidate set.

This attribution explains *why* multiple landing candidates are consistently penalized in this scene: although geometrically feasible, they violate explicit stand-off requirements with respect to nearby people, obstacles, or structural boundaries. Crucially, the provenance-based analysis renders the decision process transparent and actionable. Safety engineers can (i) *inspect* which declared safety constraints are violated by each candidate, (ii) *trace and replay* the exact reasoning paths during debugging or certification review, and (iii) *adapt* policy behavior by modifying symbolic parameters (e.g., the radius in near_to) without retraining any neural component. By contrast, purely learning-based approaches typically expose only aggregate outputs or confidence scores, offering limited insight into *which* safety constraints are violated and weak support for systematic analysis under distributional shift.

4.5 Discussion

The scope of this work is *safe landing assessment* rather than full autonomous landing execution. Accordingly, our evaluation focuses on assessing landing-site suitability instead of closed-loop flight control or touchdown dynamics. Simulation is used as the primary evaluation environment, as it enables controlled and repeatable testing across a diverse range of scenarios that would be impractical or unsafe to reproduce systematically in real-world field trials. Hardware-in-the-loop (HIL) experiments complement simulation by confirming that the complete pipeline executes on target edge hardware with competitive latency and system-level metrics (e.g., CPU/GPU utilization, memory, and power), which are key considerations for real-world deployment engineers.

The curated set of 72 landing images (augmented with synthetic edge cases) is used *only* to distil explicit symbolic safety rules through human-in-the-loop neuro-symbolic synthesis, not to train perception models or learn label alignments. These images cover diverse safety-relevant semantics-person (71%), vehicle (20%), obstacles (46%), water (42%), paved (85%), dirt (27%), grass (54%), and roofs (46%) and serve to expose the LLM to representative safety concepts rather than scene-specific layouts. Generalisation is evaluated on an independent and substantially different test set of 72 landing scenarios. None of these scenarios are used during reasoning-engine construction. To quantify the distribution gap, we compute distances in a ResNet-50 embedding space, observing clear separation between construction and test sets (Wasserstein distance 3.44, mean 1.91, std 3.09), indicating that the learned symbolic rules capture general safety principles (e.g., clearance and non-intersection) rather than memorising visual layouts.

Human involvement in the synthesis of the Scallop-based reasoning engine is intentionally minimal. Domain experts interact only with simulation execution results derived from pre-generated symbolic world models, inspecting the dominant contributing rules rendered in human-readable form to provide high-level feedback. This feedback is translated into prompt updates for rule synthesis and typically converges within at most two iterations, without requiring manual rule authoring or low-level tuning during deployment.

Our simulation scenarios are informed by prior industry collaborations on drone delivery, emergency response, and landing operations, grounding the evaluation in realistic use cases. However, they do not yet cover the full spectrum of mission types or environmental complexity. In particular, the current scenarios contain limited dynamic elements (e.g., moving people or vehicles), which constrains the extent to which the explicit world model and reasoning engine can exploit richer symbolic representations and rules. We expect that more complex and dynamic scenarios would further highlight the advantages of explicit world modeling and symbolic reasoning over state-of-the-art implicit approaches. Future work-especially in collaboration with large-scale operators such as Amazon Prime Air and Google Wing-will expand evaluation to more diverse and challenging settings, including scenarios generated via online adaptive testing to expose rare and safety-critical edge cases [35]. Another complementary research direction is to incorporate additional sensing modalities beyond the single downward-facing camera used in this study, reflecting the evolution of industrial platforms toward richer perception capabilities.

The symbolic world model relies on a predefined taxonomy derived from an existing large-scale drone landing dataset. Although this taxonomy captures common landing-relevant concepts, it may not be exhaustive. With broader industry involvement, the taxonomy can be extended, and we are exploring adaptive and hierarchical rule mechanisms that construct explicit world models without requiring a fixed, manually specified taxonomy.

Finally, unlike recent foundation-model-centric approaches that derive scene representations implicitly from pre-trained/fine-tune foundation models such as CLIP (e.g., LASER [28], ESCA [29]), our scenario graph and world model construction are fully explicit and symbolic. The reasoning layer is expressed in first-order logic, making it amenable to static analysis and formal verification using established tools (e.g., Isabelle/HOL [44]). Formally verifying landing-site selection against temporal safety specifications, such as linear temporal logic, is a natural next step and part of our ongoing work.

5 Conclusion and Future Work

This paper presented NeuroSymLand, a neuro-symbolic framework for *safe landing assessment (SLA)* in UAV systems that combines learning-based perception with Scallop-based probabilistic first-order logic to enable explicit, mission-conditioned reasoning. A key novelty is the introduction of an *explicit symbolic world model*, realized as a lightweight *Probabilistic Symbolic Scene Graph (PSSG)*, which abstracts task-relevant spatial and semantic structure from perception model outputs rather than relying on foundation-model generation. On top of this world model, NeuroSymLand employs a *dedicated symbolic reasoning engine*-implemented in Scallop-that evaluates landing candidates through verifiable first-order logic rules whose priorities can be dynamically adapted to different mission objectives (e.g., emergency, rescue, and conservative safe landing). By decoupling perception from safety reasoning, the framework avoids treating landing as a monolithic prediction problem and instead supports interpretable, testable, and mission-aware decision making. Across simulation-based evaluation on 72 scenarios and hardware-in-the-loop experiments, NeuroSymLand consistently demonstrates improved landing assessment quality relative to learning-based and foundation-model baselines while maintaining practical computational efficiency on edge hardware. Detailed provenance analysis further reveals how individual safety rules contribute to final decisions, and shows that the symbolic reasoning layer introduces negligible overhead compared to perception and graph construction, confirming that explicit world modeling and reasoning can be integrated into time-sensitive UAV pipelines without sacrificing deployability.

Our analysis also exposes clear boundaries of the current approach. Failure cases primarily arise from systematic semantic errors in perception, underscoring that reasoning reliability is fundamentally constrained by the quality of perceptual abstractions. This observation motivates several directions for future research. First, *deeper neuro-symbolic binding*: strengthening the alignment between symbolic concepts (e.g., *roof*, *ground*, *flat terrain*) and latent representations in VLM/LLM-based perception models, enabling

reasoning layers to detect and mitigate semantic inconsistencies rather than inherit them. Second, *temporal and contextual reasoning*: extending SLA beyond single-frame analysis to incorporate short-horizon temporal cues and relational changes that inform landing safety under dynamic conditions. Third, *uncertainty-aware and multimodal reasoning*: integrating complementary sensing modalities and propagating perception uncertainty into symbolic reasoning to support conservative decision making when confidence is low.

While this work focuses on UAV landing-site safety assessment, it highlights a world-model–plus–reasoning paradigm that is potentially relevant to other mobile and embedded systems operating in public spaces, such as delivery robots, autonomous inspection platforms, and intelligent infrastructure monitoring. Overall, NeuroSymLand illustrates how coupling explicit world modeling with neuro-symbolic reasoning can support transparent, interpretable, and mission-aware safety assessment in embedded mobile systems under realistic operating constraints.

References

[1] 2024. Phi-3.5-Vision-Instruct Model Card. https://huggingface.co/microsoft/Phi-3.5-vision-instruct.

[2] Marah Abdin et al. 2024. Phi-3 Technical Report: A Highly Capable Language Model Locally on Your Phone. arXiv:2404.14219 [cs.CL] doi:10.48550/arXiv.2404.14219

[3] Fateme Aghaee and Hamid Reza Shaker. 2025. RB-LLM Control: an Intelligent Control Framework with Rule-Based LargeLanguage Model Decision-Making. *Aerospace Science and Technology* (2025), 111259.

[4] Michael Ahn, Anthony Brohan, et al. 2022. Do As I Can, Not As I Say: Grounding Language in Robotic Affordances. arXiv:2204.01691 [cs.RO] https://arxiv.org/abs/2204.01691

[5] Saeed Hamood Alsamhi, Alexey V Shvetsov, et al. 2022. UAV computing-assisted search and rescue mission framework for disaster and harsh environment mitigation. *Drones* 6, 7 (2022), 154.

[6] Elissa M. Aminoff, Kestutis Kveraga, and Moshe Bar. 2013. The role of the parahippocampal cortex in cognition. *Trends in Cognitive Sciences* 17, 8 (2013), 379–390. doi:10.1016/j.tics.2013.06.009

[7] Bazeela Banday, Chandan Kumar Sah, and Jishnu Keshavan. 2025. Event-Based Adaptive Koopman Framework for Optic Flow-Guided Landing on Moving Platforms. arXiv preprint. arXiv:2501.16868 [cs.RO] doi:10.48550/arXiv.2501.16868

[8] Diego Ortiz Barbosa, Mohit Agrawal, Yash Malegaonkar, Luis Burbano, Axel Andersson, György Dán, Henrik Sandberg, and Alvaro A. Cardenas. 2025. Drones that Think on their Feet: Sudden Landing Decisions with Embodied AI. arXiv preprint. arXiv:2510.00167 [cs.RO] doi:10.48550/arXiv.2510.00167

[9] Diego Ortiz Barbosa, Luis Burbano, Siwei Yang, Zijun Wang, Alvaro A Cardenas, Cihang Xie, and Yinzhi Cao. 2024. Robust and efficient ai-based attack recovery in autonomous drones. In *GENZERO workshop*. Springer, 12–20.

[10] Diego Ortiz Barbosa, Luis Burbano, Siwei Yang, Zijun Wang, Alvaro A. Cardenas, Cihang Xie, and Yinzhi Cao. 2026. Robust and Efficient AI-Based Attack Recovery in Autonomous Drones. In *Proceedings of 1st GENZERO Workshop (GENZERO 2024)*, M. Andreoni and S. Thakkar (Eds.). 12–20. doi:10.1007/978-981-95-1050-4_2

[11] Francesco Betti Sorbelli. 2024. UAV-based delivery systems: A systematic review, current trends, and research challenges. *Journal on Autonomous Transportation Systems* 1, 3 (2024), 1–40.

[12] Haechan Mark Bong, Rongge Zhang, Alexandre Robillard, and Giovanni Beltrame. 2025. PEACE: Prompt Engineering Automation for CLIPSeg Enhancement for Safe-Landing Zone Segmentation. In *2025 IEEE/RSJ International Conference on Intelligent Robots and Systems (IROS)*. doi:10.1109/IROS60139.2025.11246443

[13] G. Bradski. 2000. The OpenCV Library. *Dr. Dobb's Journal of Software Tools* (2000).

[14] Siwei Cai, Yuwei Wu, and Lifeng Zhou. 2025. LLM-Land: Large Language Models for Context-Aware Drone Landing. arXiv preprint. arXiv:2505.06399 [cs.RO] doi:10.48550/arXiv.2505.06399

[15] Miguel Angel Cerda, Jonathan Flores, Sergio Salazar, Iván González-Hernández, and Rogelio Lozano. 2025. Depth-Based Safe Landing for Unmanned Aerial Vehicles in GPS-Denied Environment. *Drones* 9, 11 (2025), 764. doi:10.3390/drones9110764

[16] Jie Chen, Weiming Du, et al. 2024. Emergency uav landing on unknown field using depth-enhanced graph structure. *T-ASE* (2024).

[17] Xuecheng Chen, Haoyang Wang, Zuxin Li, Wenbo Ding, Fan Dang, Chengye Wu, and Xinlei Chen. 2023. DeliverSense: Efficient Delivery Drone Scheduling for Crowdsensing with Deep Reinforcement Learning *(UbiComp/ISWC '22 Adjunct)*. Association for Computing Machinery, New York, NY, USA, 403–408. doi:10.1145/3544793.3560412

[18] William W. Cohen. 2016. TensorLog: A Differentiable Deductive Database. *arXiv preprint arXiv:1605.06523* (2016). https://arxiv.org/abs/1605.06523

[19] Chiranjivi Dahal, Hari Bahadur Dura, and Laxman Poudel. 2021. Design and Analysis of Propeller for High-Altitude Search and Rescue Unmanned Aerial Vehicle. *International Journal of Aerospace Engineering* 2021, 1 (2021), 6629489.

[20] Luc De Raedt, Angelika Kimmig, and Hannu Toivonen. 2007. ProbLog: A Probabilistic Prolog and Its Application in Link Discovery. In *IJCAI*. Hyderabad, India, 2462–2467.

[21] Didula Dissanayaka, Thumeera R Wanasinghe, Oscar De Silva, Awantha Jayasiri, and George KI Mann. 2023. Review of navigation methods for UAV-based parcel delivery. *IEEE Transactions on Automation Science and Engineering* 21, 1 (2023), 1068–1082.

[22] Xin Dong, Huadong Li, Yangjie Cui, Jinwu Xiang, Daochun Li, and Zhan Tu. 2024. Aerial Landing of Micro UAVs on Moving Platforms Considering Aerodynamic Interference. *IEEE Robotics and Automation Letters* 9, 11 (2024), 10089–10096. doi:10.1109/LRA.2024.3466093

[23] Luyu Gao, Aman Madaan, Shuyan Zhou, Uri Alon, Pengfei Liu, Yiming Yang, Jamie Callan, and Graham Neubig. 2023. PAL: Program-aided Language Models. arXiv:2211.10435 [cs.CL] https://arxiv.org/abs/2211.10435

[24] Sergio Garrido-Jurado, Rafael Muñoz-Salinas, Francisco J. Madrid-Cuevas, and Manuel J. Marín-Jiménez. 2014. Automatic generation and detection of highly reliable fiducial markers under occlusion. *Pattern Recognition* 47, 6 (2014), 2280–2292. doi:10.1016/j.patcog.2014.01.005

[25] Timo Hinzmann, Thomas Stastny, Cesar Cadena, Roland Siegwart, and Igor Gilitschenski. 2018. Free LSD: Prior-Free Visual Landing Site Detection for Autonomous Planes. *IEEE Robotics and Automation Letters* 3, 3 (2018), 2545–2552. doi:10.1109/LRA.2018.2809962

[26] Hann Woei Ho, Guido C. H. E. de Croon, Erik van Kampen, Qiping P. Chu, and Max Mulder. 2018. Adaptive Gain Control Strategy for Constant Optical Flow Divergence Landing. *IEEE Transactions on Robotics* 34, 2 (2018), 508–516. doi:10.1109/TRO.2018.2817418

[27] Jiani Huang, Ziyang Li, et al. 2021. Scallop: From Probabilistic Deductive Databases to Scalable Differentiable Reasoning. In *Advances in Neural Information Processing Systems (NeurIPS 2021)*.

[28] Jiani Huang, Ziyang Li, Mayur Naik, and Ser-Nam Lim. 2025. LASER: A Neuro-Symbolic Framework for Learning Spatio-Temporal Scene Graphs with Weak Supervision. In *The Thirteenth International Conference on Learning Representations*.

[29] Jiani Huang, Amish Sethi, Matthew Kuo, Mayank Keoliya, Neelay Velingker, JungHo Jung, Ser-Nam Lim, Ziyang Li, and Mayur Naik. 2025. ESCA: Contextualizing Embodied Agents via Scene-Graph Generation. In *The Thirty-ninth Annual Conference on Neural Information Processing Systems*.

[30] Shumaila Javaid, Hamza Fahim, Bin He, and Nasir Saeed. 2024. Large language models for uavs: Current state and pathways to the future. *IEEE Open Journal of Vehicular Technology* (2024).

[31] Andrew E. Johnson, James F. Montgomery, and Larry H. Matthies. 2005. Vision-Guided Landing of an Autonomous Helicopter in Hazardous Terrain. In *Proceedings of the IEEE International Conference on Robotics and Automation (ICRA)*. 3966–3971.

[32] Seunghyun Lee, Babar Shahzaad, Balsam Alkouz, Abdallah Lakhdari, and Athman Bouguettaya. 2023. Autonomous Delivery of Multiple Packages Using Single Drone in Urban Airspace *(UbiComp/ISWC '22 Adjunct)*. Association for Computing Machinery, New York, NY, USA, 3 pages. doi:10.1145/3544793.3560330

[33] Xueping Li, Jose Tupayachi, Aliza Sharmin, and Madelaine Martinez Ferguson. 2023. Drone-aided delivery methods, challenge, and the future: A methodological review. *Drones* 7, 3 (2023), 191.

[34] Jacky Liang, Wenlong Huang, et al. 2023. Code as Policies: Language Model Programs for Embodied Control. arXiv:2209.07753 [cs.RO] https://arxiv.org/abs/2209.07753

[35] Linfeng Liang, Yao Deng, Kye Morton, Valtteri Kallinen, Alice James, Avishkar Seth, Endrowednes Kuantama, Subhas Mukhopadhyay, Richard Han, and Xi Zheng. 2025. GARL: Genetic Algorithm-Augmented Reinforcement Learning to Detect Violations in Marker-Based Autonomous Landing Systems. In *2025 IEEE/ACM 47th International Conference on Software Engineering (ICSE)*. IEEE Computer Society, 613–613.

[36] John W. Lloyd. 1987. *Foundations of Logic Programming* (2 ed.). Springer, Berlin, Heidelberg. doi:10.1007/978-3-642-83189-8

[37] Gabriel Loureiro, André Dias, Alfredo Martins, and José Almeida. 2021. Emergency landing spot detection algorithm for unmanned aerial vehicles. *Remote Sensing* 13, 10 (2021), 1930.

[38] Piotr Łuczak and Grzegorz Granosik. 2025. Autonomous UAV Landing and Collision Avoidance System for Unknown Terrain Utilizing Depth Camera with Actively Actuated Gimbal. *Sensors* 25, 19 (2025), 6165. doi:10.3390/s25196165

[39] Yuebin Lun, Honglun Wang, et al. 2022. Target search in dynamic environments with multiple solar-powered UAVs. *TVT* 71, 9 (2022), 9309–9321.

[40] Robin Manhaeve, Sebastijan Dumančić, Angelika Kimmig, Thomas Demeester, and Luc De Raedt. 2018. DeepProbLog: Neural Probabilistic Logic Programming. In *Advances in Neural Information Processing Systems (NeurIPS)*.

[41] Alina Marcu, Dragos Costea, Vlad Licaret, Mihai Pîrvu, Emil Slusanschi, and Marius Leordeanu. 2018. SafeUAV: Learning to estimate depth and safe landing areas for UAVs from synthetic data. In *ECCV Workshops*. 0–0.

[42] Ahmad Merei, Hamid Mcheick, Alia Ghaddar, and Giovanni Beltrame. 2025. ESLS: A Vision-Based Emergency Safe Landing System for UAVs. *Procedia Computer Science* 272 (2025), 277–285. doi:10.1016/j.procs.2025.10.206

[43] Mayank Mittal, Rohit Mohan, Wolfram Burgard, and Abhinav Valada. 2019. Vision-based autonomous UAV navigation and landing for urban search and rescue. In *The International Symposium of Robotics Research*. Springer, 575–592.

[44] Tobias Nipkow, Markus Wenzel, and Lawrence C Paulson. 2002. *Isabelle/HOL: a proof assistant for higher-order logic*. Springer.

[45] Institute of Engineering Geodesy and Graz University of Technology Measurement Systems (IGMS). [n. d.]. Semantic Drone Dataset. https://www.tugraz.at/index.php?id=22387.

[46] Edwin Olson. 2011. AprilTag: A robust and flexible visual fiducial system. In *2011 IEEE International Conference on Robotics and Automation (ICRA)*. IEEE, 3400–3407. doi:10.1109/ICRA.2011.5979561

[47] OpenAI. 2025. ChatGPT: O3-Mini. https://openai.com/chatgpt. Large language model.

[48] Francis D. Raslau et al. 2015. Memory Part 2: The Role of the Medial Temporal Lobe. *Radiographics* (2015). Available via PubMed Central: PMC7990589.

[49] Cynthia Rudin. 2019. Stop explaining black box machine learning models for high stakes decisions and use interpretable models instead. *Nature Machine Intelligence* 1, 5 (2019), 206–215. doi:10.1038/s42256-019-0048-x

[50] Srikanth Saripalli, James F. Montgomery, and Gaurav S. Sukhatme. 2003. Visually-Guided Landing of an Unmanned Aerial Vehicle. *IEEE Transactions on Robotics and Automation* 19, 3 (2003), 371–380.

[51] Kirk Y. W. Scheper and Guido C. H. E. de Croon. 2020. Evolution of Robust High-Speed Optical-Flow-Based Landing for Autonomous Micro Air Vehicles. *Robotics and Autonomous Systems* 124 (2020), 103380. doi:10.1016/j.robot.2019.103380

[52] Pascal Schoppmann, Pedro F Proença, Jeff Delaune, Michael Pantic, Timo Hinzmann, Larry Matthies, Roland Siegwart, and Roland Brockers. 2021. Multi-resolution elevation mapping and safe landing site detection with applications to planetary rotorcraft. In *2021 IEEE/RSJ International Conference on Intelligent Robots and Systems (IROS)*. IEEE, 1990–1997.

[53] Mattia Secchiero, Nishanth Bobbili, Yang Zhou, and Giuseppe Loianno. 2024. Visual Environment Assessment for Safe Autonomous Quadrotor Landing. In *2024 International Conference on Unmanned Aircraft Systems (ICUAS)*. 807–813. doi:10.1109/ICUAS60882.2024.10557078

[54] Shital Shah, Debadeepta Dey, Chris Lovett, and Ashish Kapoor. 2018. Airsim: High-fidelity visual and physical simulation for autonomous vehicles. In *Field and Service Robotics: Results of the 11th International Conference*. Springer, 621–635.

[55] Zhuoyue Tan, Boyong He, Yuxiang Ji, and Liaoni Wu. 2025. VisLanding: Monocular 3D Perception for UAV Safe Landing via Depth-Normal Synergy. In *Proceedings of the IEEE/RSJ International Conference on Intelligent Robots and Systems (IROS)*.

[56] John Wang and Edwin Olson. 2016. AprilTag 2: Efficient and robust fiducial detection. In *2016 IEEE/RSJ International Conference on Intelligent Robots and Systems (IROS)*. Daejeon, South Korea.

[57] Enze Xie, Wenhai Wang, Zhiding Yu, Anima Anandkumar, Jose M. Alvarez, and Ping Luo. 2021. SegFormer: Simple and Efficient Design for Semantic Segmentation with Transformers. arXiv:2105.15203 [cs.CV] https://arxiv.org/abs/2105.15203

[58] Xi Ye, Qiaochu Chen, Isil Dillig, and Greg Durrett. 2023. SatLM: Satisfiability-Aided Language Models Using Declarative Prompting. arXiv:2305.09656 [cs.CL] https://arxiv.org/abs/2305.09656

[59] Haoren Zheng, Syeda Amna Rizvi, Muhammad Umair, and Athman Bouguettaya. 2026. Managing Drone Traffic in Urban Skyway Networks *(UbiComp Companion '25)*. Association for Computing Machinery, New York, NY, USA, 399–402. doi:10.1145/3714394.3754420